JOURNAL OF MATERIALS RESEARCH AND TECHNOLOGY 2022;19:472–506

Available online at www.sciencedirect.com

jmr&t Journal of Materials Research and Technology

journal homepage: www.elsevier.com/locate/jmrt

Review Article

# Relevant aspects of laser cutting of NiTi shape memory alloys

C.A. Biffi*, J. Fiocchi, A. Tuissi

*National Research Council, Institute of Condensed Matter Chemistry and Technologies for Energy, Unit of Lecco, CNR ICMATE, Via G. Previati 1E, 23900 Lecco, Italy*

ARTICLE INFO

*Article history:*
Received 24 February 2022
Accepted 24 March 2022
Available online 29 April 2022

*Keywords:*
Laser material processing
Laser cutting
Shape memory alloy
NiTi
Microstructure
Functional properties
Devices
Stents

ABSTRACT

Since several years the need for realizing small and smart devices composed of functional materials is constantly increasing. Among this advanced materials, shape memory alloys (SMAs) are some of the most important functional materials in several applications, including in the biomedical and aerospace fields. Nowadays, laser cutting is probably the most widespread cutting technology for realising SMA mini- and micro-devices for several applications. The present manuscript reviews the scientific literature on the performance of laser-cut elements, in NiTi SMA, under different points of view. The literature was systematically analysed, according with a technological, metallurgical, functional and device/prototypal approaches. It can be highlighted that a relevant correlation between design, process condition and material performances can promote the realization of advanced smart devices made in NiTi SMA.



## 1. Introduction

The demand for and use of advanced engineering and smart materials, which can enhance the performance of common devices and realise novel and high-tech products, are among the most important reasons for the diffusion of unconventional and advanced processes. Among advanced manufacturing methods, laser beam machining (LBM) is widely used in several applications because the generated radiation can be absorbed by almost all engineering materials [1]. The laser beam can easily be shaped in the spatial and temporal domains to cover numerous processes, such as cutting, welding, heat treatments, drilling, surface texturing, marking, material deposition, and additive manufacturing. The possibility of focusing the beam energy in a very limited area and the resulting limited modification of the material properties makes these processes highly suitable and promising for materials that are sensitive to temperature variations [2]. In particular, LBM can be modulated to realise macro-and micro-products [3], which is an additional advantage of this advanced manufacturing process for the production of small, smart, and high-tech devices.

Among metals, shape memory alloys (SMAs) are likely the most sensitive to temperature changes. SMAs are functional materials that are characterised by two peculiar properties: pseudoelasticity (PE) and shape memory effect (SME) [4,5].

* Corresponding author.
E-mail address: carloalberto.biffi@cnr.it (C.A. Biffi).
https://doi.org/10.1016/j.jmrt.2022.03.146

These features exist due to a reversible solid-state phase transformation, indicated by martensitic transformation (MT). SMAs have drawn significant attention in recent years in a broad range of commercial and scientific applications owing to their unique and superior properties [6]. However, the production and processing of SMAs can significantly affect the final performance of the devices in which they are employed; therefore, clarification of the effects of machining is fundamental for all SMA applications [7–10].

In this light, this paper reviews the scientific literature on laser cutting of NiTi SMAs; as a multidisciplinary approach must be undertaken for deep understanding of the mechanisms involved during laser absorption and heat conduction, the effects of the main process parameters, main characteristics of the realised kerf, and functional behaviours of the SMA elements after laser cutting are discussed. In addition, a literature survey was conducted on the principal applications, which are associated with the most well-known patents and represent aspects of fundamental interest in industry. In particular, the initial sections of this report address some preliminary concepts regarding the properties of the greatest interest of SMAs, first NiTi and NiTi-based alloys, and then commercially unavailable SMAs, and the principal aspects and mechanisms involved in laser cutting. Thereafter, the state-of-the-art laser cutting of SMAs are presented from technological, microstructural, and functional perspectives. Finally, the latest challenges and opportunities associated with laser cutting of SMAs for realising devices and prototypes are discussed.

## 2. NiTi SMA overview: functional behaviour and industrial applications

SMAs constitute a particular class of functional materials that exhibit peculiar properties not found in other materials. These extraordinary properties are the SME and superelasticity (SE) [4]. These unique thermomechanical properties are due to a reversible solid-state phase transformation between a high-temperature parent phase (B2, austenite) and a low-temperature product phase (B19′, martensite). Austenite and martensite are characterised by body-centred cubic and monoclinic crystal structures, respectively. This phase transformation is called thermo-elastic MT and can be activated in two different ways, as shown in Fig. 1: (i) by a temperature change in the case of thermally induced martensite or (ii) through the application of a mechanical load in the case of stress-induced martensite (SIM).

When the austenitic structure is cooled down, thermally induced MT (B2→B19′) occurs in the range between the martensite starting temperature (Ms) and martensite finishing temperature (Mf). In contrast, when the martensitic structure is heated, the reverse transformation between martensite and austenite (B19′→B2) occurs in the range between the austenite

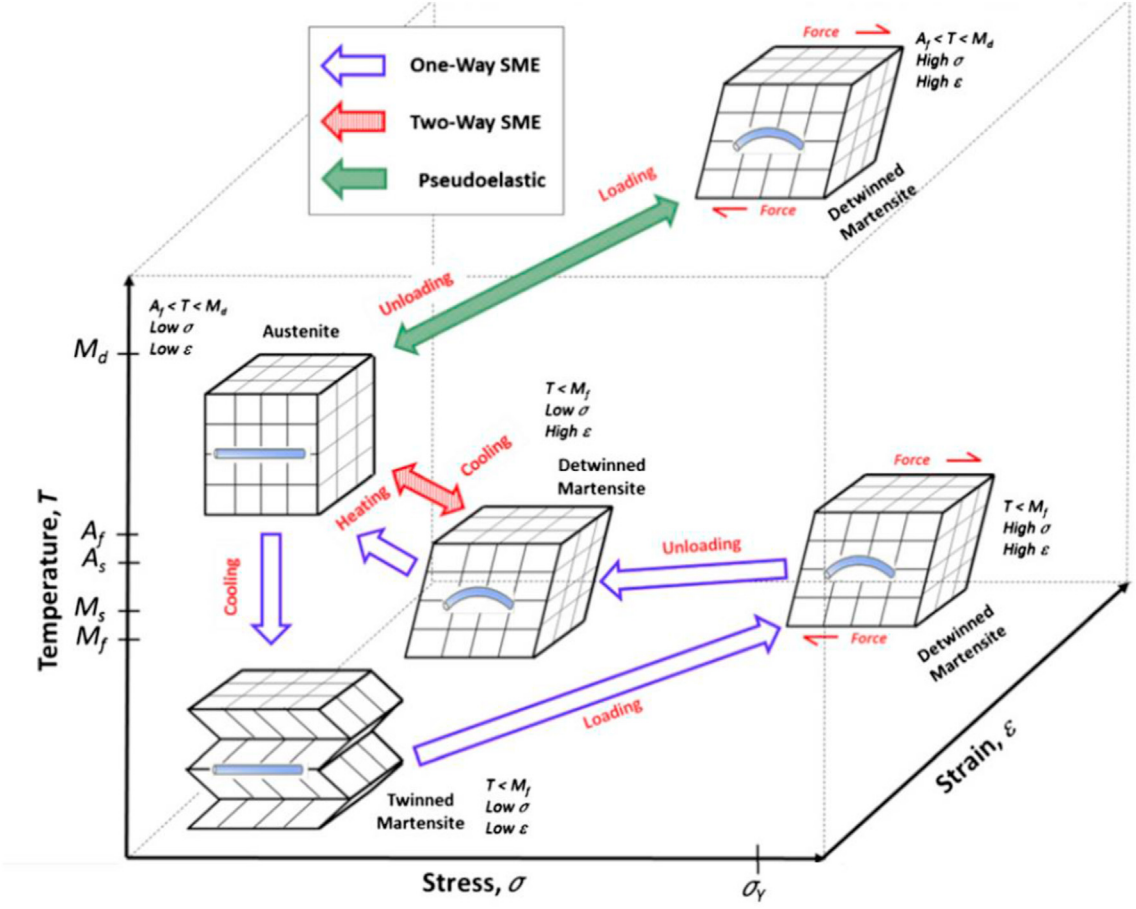


**Fig. 1 – Overview of the phase transformations involved in SMAs [6].**

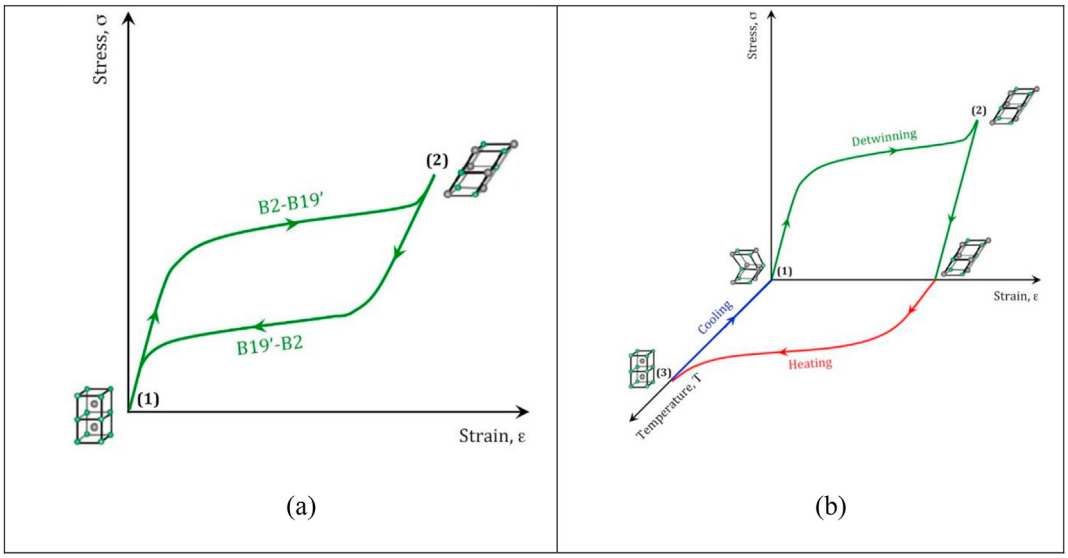


**Fig. 2 – Stress–strain curve of an austenitic NiTi alloy with characteristic transformation stresses (a) and the corresponding thermo-mechanical response (b), showing the SME [14].**

starting temperature (As) and austenite finishing temperature (Af). These characteristic transformation temperatures are related to the alloy composition [9] and thermo-mechanical processing conditions [11–13]. MT can also be induced by applying an external load. When a mechanical load is applied to the austenitic structure, the stress-induced B2→B19′ transformation occurs, giving rise to a plateau in the stress–strain curve of the alloy, as shown in Fig. 2. If the mechanical load is removed, the reverse B19′→B2 transformation occurs, which is related to another stress plateau that occurs at a lower stress, and almost complete strain recovery is allowed. This high strain recovery capability (up to 8%–10%) observed during isothermal loading/unloading conducted at temperatures above Af is the so-called superelastic or pseudoelastic effect (PE). It is evident that the so-called pseudoelastic flag, as shown in Fig. 2a, caused by reversible stress-induced MT, can be used to produce flexible devices for biomedical applications, such as stents or orthodontic wires.

The SME can be described with reference to the phase-transition mechanism shown in Fig. 2b. The element is loaded and deformed at low temperatures in the martensitic phase (below Mf). After unloading, a significant unrecoverable strain, caused by the accumulation of dislocations, remains, as in traditional materials. However, in SMAs, heating above the Af induces the reverse MT, and the obtained fully austenitic structure enables the recovery of the previous residual strain, and the original shape of the SMA element is regained [4]. Consequently, materials that exhibit SME only upon heating can be used as actuators or sensors because of the mechanical work generated upon temperature change once an external load is applied.

Among SMAs, the near-equiatomic NiTi binary system shows the most exploitable characteristics owing to its high stress and strain recovery capabilities and stable functional properties. NiTi-based SMAs are usually called Nitinol, due to their composition and discovery at the Naval Ordinance Laboratory (NOL) in the 1960s [15]. Currently, NiTi-based SMAs provide the best combination of properties for the most important commercial applications [10]. The excess Ni or Ti in NiTi alloys has a moderate solubility range, and such alloys exhibit ductility comparable to that of most ordinary alloys. One of the most exploited properties of Nitinol is its high biomechanical compatibility, and its extraordinary compliance with biological materials (see Fig. 3) makes it one of the most suitable metals for biomedical applications, enabling reduced healing time and decreasing the trauma to the surrounding tissue [16–18]. Table 1 lists the principal properties of NiTi SMA.

Many studies have been performed to assess the effects of the chemical composition of binary NiTi alloys. Even a very limited change in the alloy composition can have a considerable effect on the transformation temperatures; in particular, Ni-rich alloys exhibit lower Ms, as depicted in Fig. 4. Ms is below room temperature for Ni-rich alloys, whereas maximum Ms values of 90–100 °C were obtained for alloys with Ni contents below 49.5% [10].

PE, which involves the ability to achieve full recovery after being deformed to strains as high as 8%, is commonly exploited in biomedical devices [16], mainly in stents [22]. Stents are among the most representative commercial products and are often machined by laser cutting from thin tubes to realise complex three-dimensional (3D) struts [23–25]. These devices are adopted as structural elements for avoiding the collapse of blood vessels, like arteries, when they are partially or completely occluded. They can be classified depending on their specific use into the human body, as well as their strut type [26]. Due to their different shapes and final functional properties, different methods of laser cutting can be also approached [27].

Fig. 5a depicts an example of an SMA stent strut, while in Fig. 5b the evolution of the stress-strain curve is represented when the stent is inserted in the vessels.

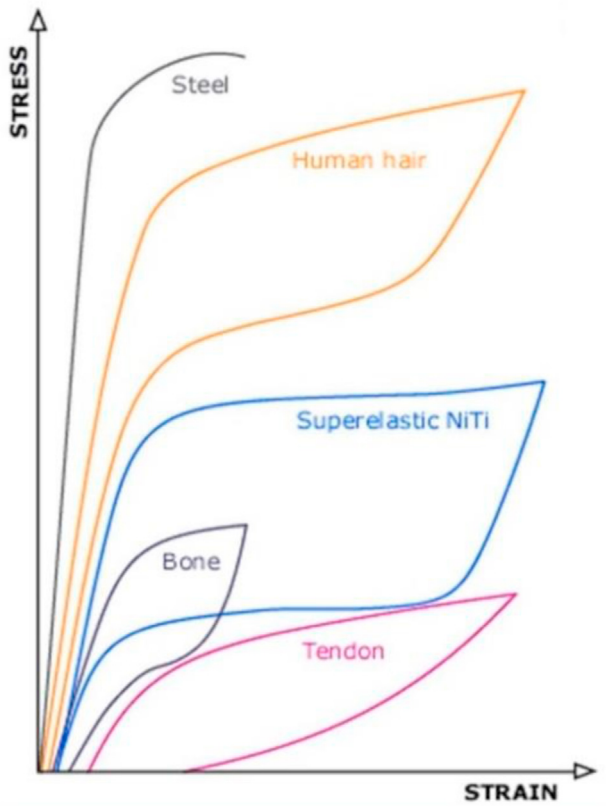


**Fig. 3 – Stress–strain curves of several natural biological materials superimposed on the Nitinol and steel stress–strain curves [16].**

Conversely, SMEs are commonly used in actuators or sensors [28] because mechanical work can be generated by heating and cooling an SMA element under an applied load. In this case, laser cutting enables the fabrication of mini- and micro-devices, which can offer high actuating frequencies as well as high power-to-weight ratios [29–31]. Fig. 6 shows a representative example of an actuator based on an SMA spring.

Literature reports also other promising SMA applications in other sectors, like the civil one [32,33], for their interesting damping capacity. Anyways, to the best knowledge of the authors' literature, no works regarding laser cutting of SMAs are present.

**Table 1 – Principal properties of NiTi SMA [19,20].**

| Properties | Unit | Values |
|---|---|---|
| Melting point | °C | 1250 |
| Fusion heat | J/cm$^3$ | 2322 |
| Density | g/cm$^3$ | 6.45 |
| Thermal conductivity | W/m K | 10–18 |
| Thermal diffusivity | cm$^2$/s | 0.125 |
| Specific heat | J/kg K | 490 |
| Dilatation coefficient | μm/k | |
| Austenite | | 11 |
| Martensite | | 6.6 |
| Young's modulus | GPa | |
| Austenite | | 70 |
| Martensite | | 30–35 |
| Yield stress | MPa | 100–400 |
| Tensile strength | MPa | 2000 |
| Reversible deformation (one-way memory effect) | % | 8 |
| Reversible deformation (two-way memory effect) | % | 3.2 |
| Corrosion resistance | | Very good |
| Biocompatibility | | Very good |

## 3. Overview of laser cutting process

### 3.1. *Laser cutting process*

Laser cutting, one of the most established laser material processing technologies, is a thermal method for shaping and separating a workpiece into segments of the desired geometry [1]. The process is performed by moving a focused laser beam on the workpiece, as shown schematically in Fig. 7a. Once absorbed, the laser beam heats up the material, locally inducing melting and potentially even vaporisation of the material itself. A flow of shielding gas, which may be inert or reactive depending on the material type, is adduced coaxially with the laser beam by a nozzle. The main objectives of the gas flow are to push away the melted material for kerf generation and to limit the thermal damage of the workpiece or material (see Fig. 7b).

The industrial configuration of the laser system used for cutting consists of a laser source, which is typically an active fibre laser, Nd:YAG, $CO_2$, or femtosecond laser, coupled with an optical chain for delivering and focusing the laser beam. In the proximity configuration (see Fig. 8a), the beam focalisation is such that the smallest beam size is obtained on the surface through a focusing head, with a coaxial nozzle for adduction of the shielding gas. Another option is remote cutting, in which the laser beam is focused and moved using a galvanometer equipment, which moves two mirrors rotating at high velocity (see Fig. 8b). Most literature reports results based on the use of proximity cutting heads, while only a few papers address the use of the remote configuration, which is typically coupled only with a femtosecond laser. However, successful laser cutting results are associated with the relative motion between the radiation beam and workpiece. Usually, the workpiece is moved using a motion stage that controls the 3D Cartesian coordinates as well as at least one rotational axis, for instance, for the cutting of stents from tubes. Fig. 9 provides an example of the laser equipment used for cutting the stents.

To realise superelastic NiTi stents, cutting is performed on tubes with outer diameters (ODs) ranging from 0.1 mm to 15 mm. In any case, additional difficulties in tube cutting are faced with respect to the processing of tapes or plates: first, the cutting surface is a curve, and second, there is a risk of damaging the internal surface of the tube opposite to the side of the laser breakthrough. This problem may be overcome by performing the process in a liquid medium.

Laser cutting can be described as a result of the cooperation and interaction between numerous variables, which can be linked to the principal process parameters (such as power, speed, laser spot size, gas flow pressure and type, beam

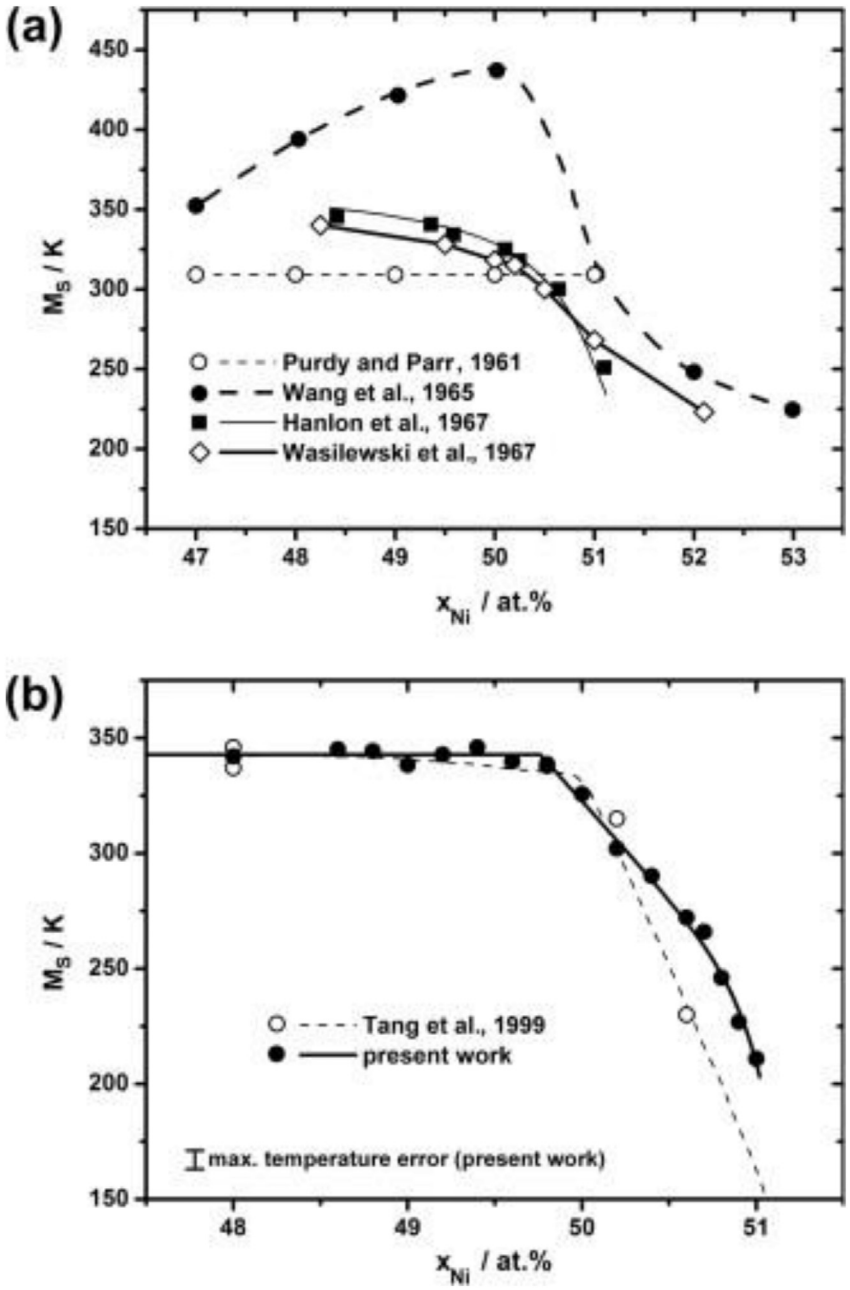


**Fig. 4 – Dependence of Ms on the Ni content in NiTi SMA [21].**

quality, and emission mode), thermo-physical properties of the material (such as thermal capacity, thermal conductivity, density, and index of refraction), and geometrical features (such as part thickness and cutting path). All these factors can significantly affect the cutting performance and consequently the quality and thermal damage of the workpiece [37].

Two principal mechanisms of material removal can be defined for metals: fusion cutting and vaporisation cutting. The first approach is characterised by predominant melting, due to a relatively low absorbed power density and long interaction time. This combination of process parameters enables intense heat conduction, generating thermal wave diffusion. The second technique is associated with the use of a significantly higher irradiance to overcome the boiling temperature, which can be achieved using ultrashort pulses, limiting the typical thermal damage in the area surrounding the kerf. In agreement with these two laser cutting mechanisms, the thermal contribution of the process can be modelled by assuming that all the beam energy has been used for melting and possibly vaporising the material during kerf generation. The thermal balance, which describes the material removal rate, under the previous hypotheses can be written in the following formula (1):

$$\frac{P \cdot A}{b \cdot h \cdot v} = \rho \cdot \left(C_p \cdot \Delta T + L_f + m' \cdot L_v\right) \quad (1)$$

The left side of Eq. (1) indicates the absorbed energy per unit volume, where P is the incident beam power; b and h are the

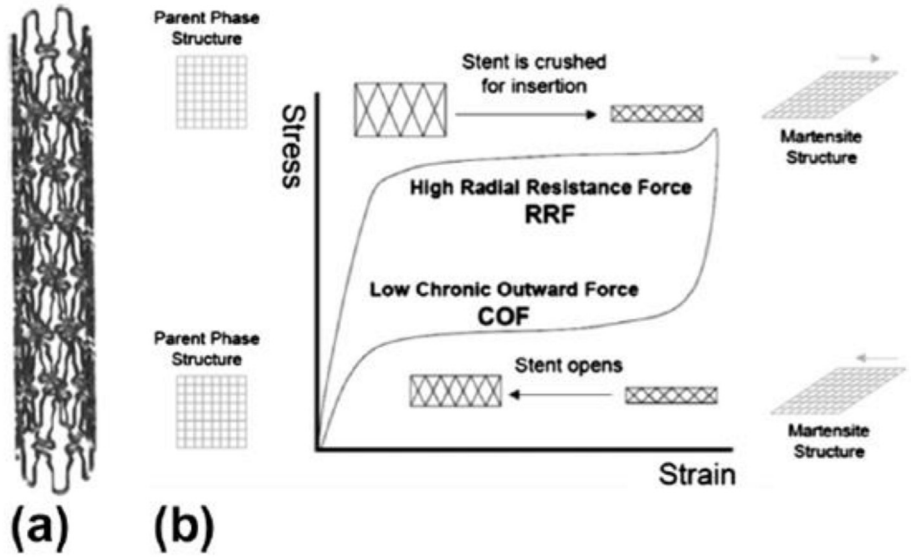


**Fig. 5 – Geometrical model of a stent realised through laser cutting (a) and superelastic response of the stent (b) [6].**

kerf width and thickness, respectively; v is the process speed; and A is the absorption coefficient. The right side of Eq. (1) represents the ideal energy needed for melting and vaporising the material, which can be determined from its thermophysical properties, where $\rho$ is the density, $C_p$ is the thermal capacity, $\Delta T$ is the difference between the initial and melting temperatures, $L_f$ is the latent heat of melting, $L_v$ is the latent heat of vaporisation, and m′ is the percentage of vaporised material. Eq. (1) demonstrates that it is possible to discriminate between fusion and vaporisation cutting, accounting for the amount of material subjected to boiling through m′.

The process operates correctly when the energy per unit volume, irradiated by the laser beam, exceeds the ideal energy for melting and possibly vaporises the material [38].

In addition to the energetic contribution of the process, the laser emission mode, specifically, continuous wave (CW) or pulse wave (PW) mode, can determine large variations in the thermal field induced by laser processing [39]. In particular, the exposure time, which is correlated to the pulse duration in the PW emission mode, should be carefully considered to optimise the microstructural and functional performance of metals.

It should also be emphasised that the laser cutting of SMAs is mainly intended for the machining of thin elements (from 0.1 mm to 1 mm in thickness), because the functional properties are enhanced in mini-scale devices [30]. It is not coincidental that in this typical thickness range, the use of PW lasers is predominant. The following paragraph remarks upon the effects of pulse durations of different ranges from the perspective of laser material processing of SMAs.

### 3.2. *Effects of pulse duration in thermal processing*

As previously reported, SMAs are very sensitive to temperature variations, and microstructural modifications can significantly affect their functional behaviour. Therefore, the evolution of the thermal field has become a fundamental issue that must be deeply understood.

The present paragraph reports the effects of the most important parameter that can influence the overheating of metals, which is the pulse duration. In fact, the pulse duration can govern the heat conduction occurring during the process, and the intensity of the thermal load on the material can be modulated by setting a pulse duration longer or shorter than the time required for heat conduction to occur. When a material is subjected to laser radiation, the absorption is localised in the skin layer. Photons are absorbed by free electrons in the surface layer in approximately 1 fs ($10^{-15}$ s). The absorbed energy is stored in the electrons during their relaxation time (approximately 1 ps = $10^{-12}$ s for metals, and approximately 1 ns = $10^{-9}$ s for plastics) [40]. After this time, the energy is converted into heat and is free to propagate through the workpiece; consequently, the electron relaxation time is equivalent to the time required to enable heat conduction. The optical penetration depth, at which the conversion from the laser energy to heat has been fully reached, is 10 nm in metals for a relaxation time of 1 ps; however, the penetration depth depends on the material properties and laser wavelength. Fig. 10 presents a schematic of the laser–matter interaction with long and ultrashort interaction times [40,41]. The fundamentals of laser–matter interaction under long pulse conditions can be described as follows: the heat transferred by the laser to the material diffuses away during the interaction time; then, the thermal front propagates under the laser beam and heat conduction becomes the predominant mechanism. This phenomenon occurs when the laser pulse duration is longer than the heat diffusion time. Heat diffusion into the surrounding material is undesirable and detrimental to the quality of machining processes associated with material removal, such as cutting, drilling, and milling. Hence, CW or PW lasers with very long pulse durations are used to perform welding, as heat conduction is a requirement

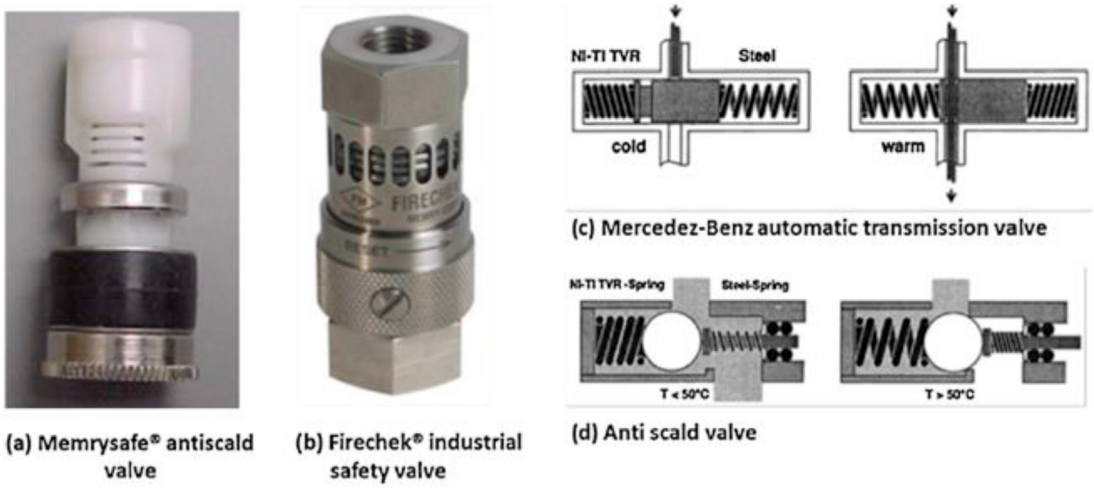


**Fig. 6 – Example of SMA actuator: safety valve (a–b) [6].**

for the coalescence of the elements to be joined. The diagram in Fig. 10a shows that the material is melted during heating, which can induce the generation of a heat-affected zone (HAZ), cracks, oxidation, and other defects. In contrast, the objective of current research on laser microprocessing of materials tends to be reducing the interaction time. When the laser pulse duration is below the critical value for heat conduction, the transmission of energy from the beam to the electronic structure of the material is different than in the previous case, which limits the propagation of the thermal front.

High peak powers (on the order of megawatts) and short pulse durations (on the order of femtoseconds) enable direct vaporisation of the material without melting. This benefit is crucial for laser processing, as the energy is concentrated sufficiently to remove only small portions of material, and there is not enough time for heat conduction. As shown in Fig. 10b, ablation is performed without heating the material surrounding the machined part, enhancing the feature quality from both morphological and microstructural perspectives. It should be emphasised that ultrashort laser pulses interact with matter in a manner that is completely different from traditional lasers with longer pulse durations [40].

When using ultrashort laser pulses, a large amount of energy is transferred rapidly to the material, which forces the material into the plasma state. The material changes from a solid to a gas, producing plasma without melting. After plasma generation on the workpiece surface, the induced pressure causes the material to expand outward from the surface in a highly energetic plume or gas. The internal forces, which previously held the material together, were insufficient to contain the expansion of ions and electrons from the surface. Consequently, no droplets condense onto the surrounding material. In addition, because a molten phase is

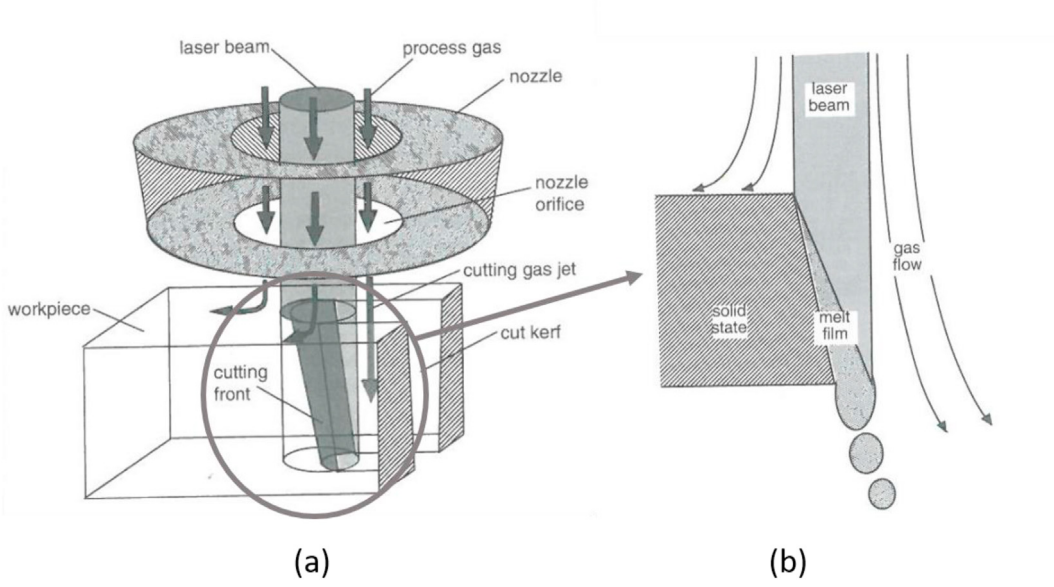


**Fig. 7 – Schematic of the laser cutting process (a) and the mechanism of material removal (b) [1].**

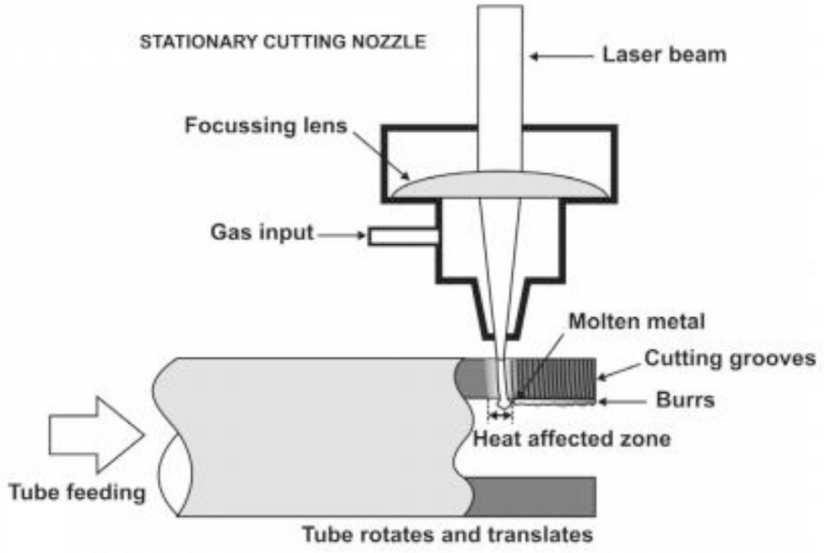


(a)

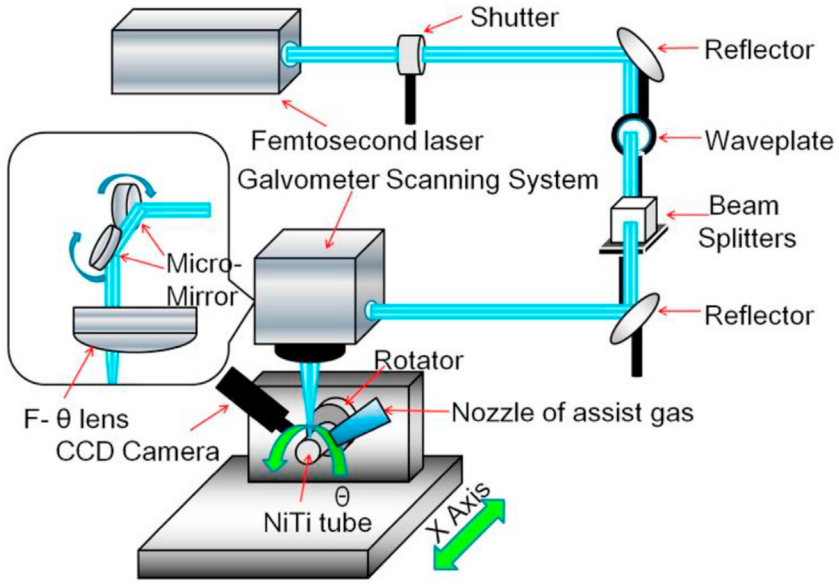


(b)

**Fig. 8 – (a) Proximity and (b) remote cutting configurations adopted for tube cutting [34,35].**

absent, there is no splattering of the material onto the surrounding surface. This operation mode is anticipated to enable the fabrication of highly accurate micromachined parts, which cannot be produced using laser pulses longer than the threshold time.

## 4. Laser cutting of NiTi SMAs

Laser cutting of NiTi SMAs has been studied for several years, thanks to the interest in utilizing Nitinol to fabricate a wide

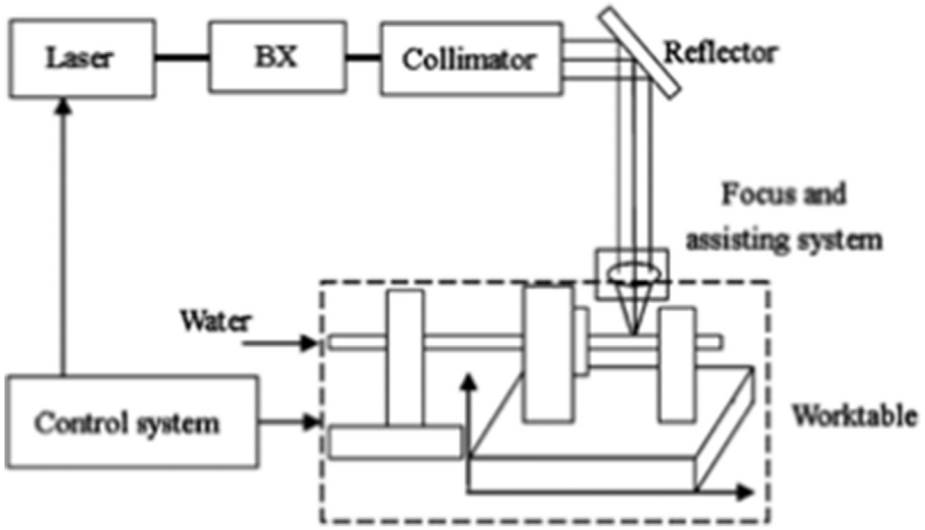


**Fig. 9 – Schematic of the laser cutting system used to fabricate a stent from a tube [36].**

variety of stents [16,42] and to realise smart sensors and actuators [43–47]. The principal advantages of laser cutting are high flexibility in forming complex shapes (i.e. thin-walled tubes for stents or micro-grippers), high productivity, and high spatial resolution, owing to its high beam-focusing ability. The principal drawback of laser processing lies in its thermal nature, which may generate microstructural modifications such as recast layers, HAZs, localised cracks, and potential chemical modifications, all of which can degrade the material properties and reduce the geometrical quality near the kerf [19,48–50]. The effect of the supplied heat during laser irradiation is strongly correlated to the sensitivity of NiTi to chemical composition changes and to its defect microstructure.

For instance, considering stent production, the laser cutting affects the formation of recast material, cracks, and local changes in the functional properties of NiTi, which are crucial during stent expansion and in terms of fatigue life. In particular, not only the recast material, but also the cracks are influenced by several process parameters, such as the shielding gas, process speed, characteristics of the laser beam, and even post-processing steps, such as sandblasting and electropolishing [51]. Further, because the high reactivity of Ti can worsen the oxidation phenomena [52] and the transformation temperature of NiTi depends significantly on the Ni/Ti composition ratio, laser processing without affecting the localised functional performance is difficult [50,51]. In the machining of thin devices, such as thin strut article stents, heat conduction can induce the formation of a large HAZ, which can affect the properties of the entire component, degrading the functional properties of the initial material [53].

Given these characteristics, the laser processing of NiTi SMAs appears more complex than that of other metallic alloys, because the feasibility of the process must be fixed not only by considering typical technological constraints (quality

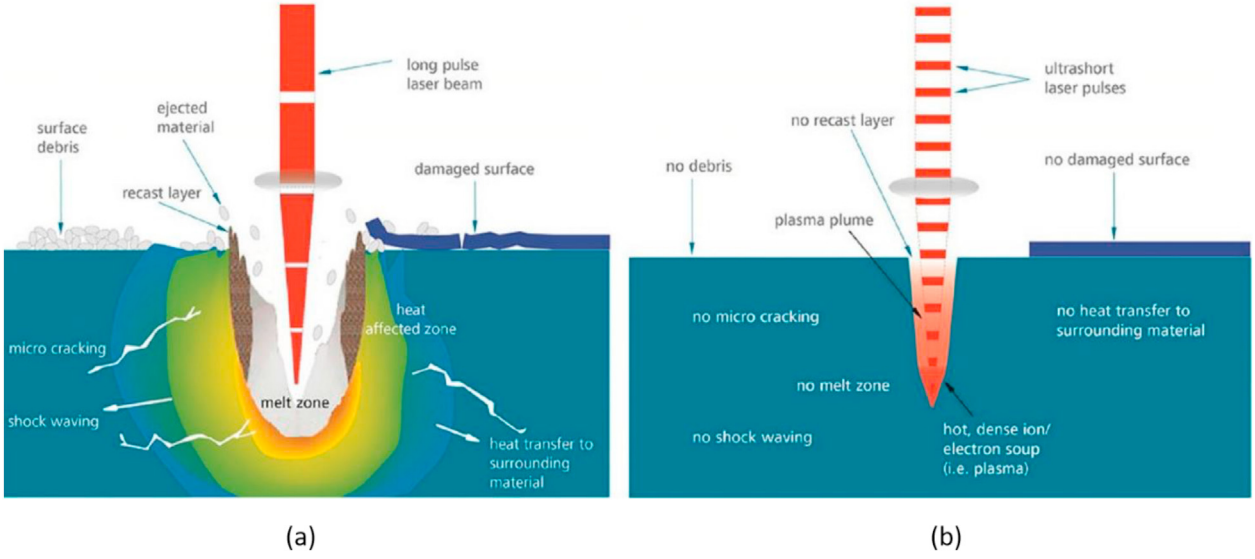


**Fig. 10 – Thermal effects during laser–matter interaction with (a) long and (b) ultrashort interaction time or pulse width [41].**

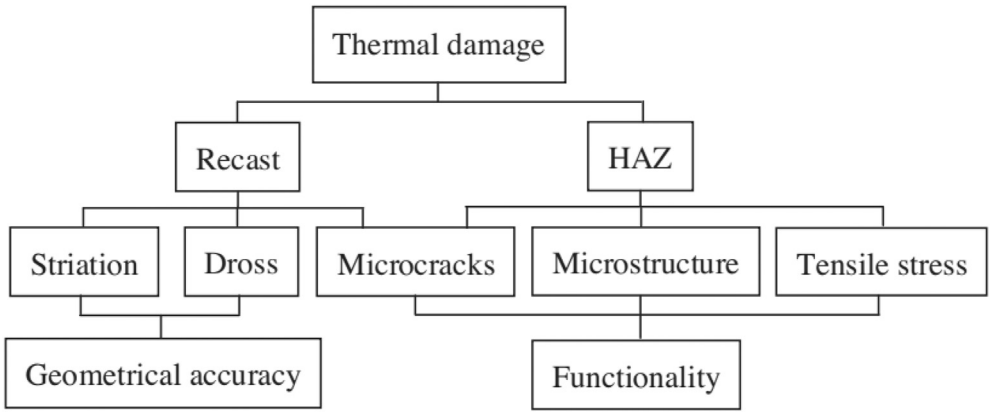


**Fig. 11 – Correlation between thermal damage in laser cutting and part functional performance [54].**

and productivity), but also by endeavouring to limit the changes in functional performance. Moreover, both the material and device performance must be considered in SMA element design. According to the papers available in the open literature regarding the laser cutting of NiTi SMAs, the following approaches can be identified:

- *Technological investigations*: The effects of the main process parameters on kerf characteristics are investigated, and the kerf width, taper, roughness, and dross formation are studied to determine the feasibility area and to optimise the process performance. In addition, attention is dedicated to different methodologies for limiting the heat diffusion into the workpiece during the cutting process.
- *Thermal modelling*: Analytical and numerical models describing the laser cutting process are discussed as support for the previous experimental approach.
- *Microstructural and functional characterisations*: The evolution of the microstructural, mechanical, and functional properties of the laser-cut material is studied.
- *Corrosion*: The corrosion behaviour of laser-cut parts is investigated, mainly from the perspective of biomedical applications.
- *Prototyping and applications*: Laser cutting technology has been demonstrated to be a precise tool for producing proof of concepts, prototypes, and small devices, which are characterised and tested.

### 4.1. *Technological investigations*

This section presents the effects of the main process parameters on kerf quality. Fig. 11 summarises the strong correlation between the heat flow associated with the specific process conditions, principal geometrical features characterising the laser-cut kerf, microstructural alterations induced in the material, and ability to modify the final part performance. In fact, it is relevant to correlate the processability, characterised by the thermal input of the process (see Eq. 1), with not only the geometrical aspects indicating the kerf quality, but also the functional performance of the SMA element.

To evaluate the laser cut quality, some criteria can be considered: burr absence or presence, roughness, dimensional accuracy, HAZ extent, and oxide generation. The kerf width can be seen as an additional criterion from the perspective of device miniaturisation, an example of which is shown in Fig. 12, and it can be controlled by achieving small laser post sizes [49].

Most literature addresses laser cutting of plates made of conventional metals. Regarding NiTi SMAs, numerous works are focused on the cutting of thin wall tubes, because the most

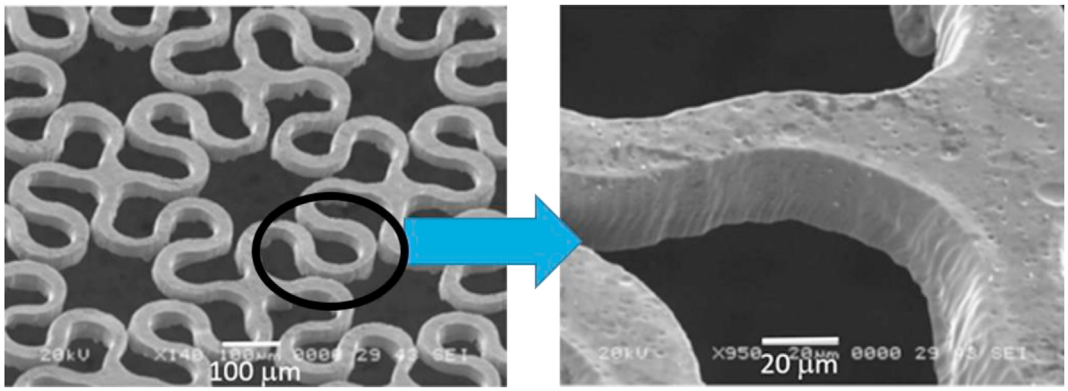


**Fig. 12 – As-cut structure in NiTi of a flat panel [49].**

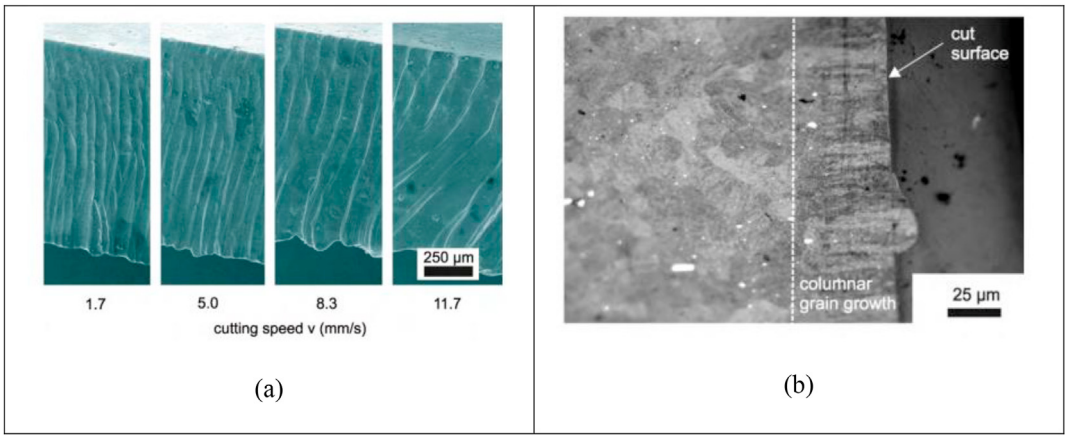


**Fig. 13 – Lateral view of the NiTi kerf, produced using a millisecond Nd:YAG laser (a) and corresponding recrystallised layer (b) [19].**

widespread NiTi components present in the market are stents. The thickness to be cut is on the order of a few hundreds of microns considering the industrial applications of NiTi, except in one study [19], in which the thickness of the investigated NiTi samples was 1 mm.

Owing to the temperature sensitivity of NiTi SMAs, the most important process parameter in laser cutting is the pulse duration. In fact, most papers have addressed the use of ultrashort pulses to limit heat conduction and thereby reduce the alteration of the microstructural and functional properties of the SMA element. However, the effects other process parameters, such as power, speed, spot size, shielding gas type, and flow, on the kerf characteristics, that is, width, taper, and dross, have also been investigated. Therefore, the following two subsections separately discuss the principal technological results achieved using long, short, and ultrashort laser pulses.

#### 4.1.1. *Effects of long and short laser pulses*

Pfeifer et al. investigated the effects of laser energy, focus position, cutting speed, and pulse duration on geometrical features such as taper, kerf width, and roughness, as well as the HAZ extension [19]. The cutting process was conducted on 1-mm-thick NiTi plates using a Nd:YAG laser source; therefore, long pulse durations (on the order of milliseconds and microseconds) were adopted to reach the high energy values required by the process. Consequently, the material removal mechanism involves pure melting. The contribution of melting is clearly visible on the lateral surface: high roughness (ranging from 10 μm to 30 μm) is typically evident, compared to that achieved by the EDM process [55]. Fig. 13a clearly depicts this feature, where the typical striations placed on the lateral surface of the kerf are visible. Such a large roughness could require post-processing to obtain components with reasonable fatigue lives. Moreover, the high thermal impact of the laser process on the SMA microstructure resulted in HAZ extension up to 30 μm, which again affected the functional properties and accuracy of the cutting process (see Fig. 13b). On the other hand, a kerf width of 15–400 μm and taper less than 2° were achieved, and the use of long pulse durations enabled us to obtain higher process speeds than are possible with ultrashort pulses, making the realisation of SMA macrodevices economic (with thickness in millimetre range and cut length in the centimetre range).

The surface quality and HAZ extension are two of the most relevant features to be minimised when cutting stents. Some researchers have analysed the effect of the principal process parameters, including the type of laser source, on these qualitative aspects. Liu et al. proposed using a pulsed active fibre laser with a pulse duration on the order of microseconds to cut thin tubes in NiTi having thicknesses of 240 μm for the production of self-expanding stents [56]. The tubes were cut by a continuous water flow through the wall of the tube to blow away the debris ejected from the cut kerf and to avoid back damage. Additionally, Ar was used as a shielding gas to protect the kerf from oxidation and to facilitate the ejection of the melted material. The combination of water flow, adduced axially to the tube, and shielding gas, adduced radially to the tube, caused the formation of a mix of ablation front and striations, which affected the final surface morphology, as depicted in Fig. 14. Similar results were obtained by Nagy et al., who observed the formation of large drops of melted material, as large as the tube thickness [57]. This formation induced large corrugations on the inner surface of the stent, indicating that a systematic study of the correlation between the process parameters and geometrical features of laser-cut kerf is of great relevance when thin-walled tubes are to be processed.

In another study, a statistical approach was implemented to investigate the degrees of association between key process parameters (laser power and cutting speed) and kerf geometry characteristics (entry/exit kerf width and taper angle), roughness, and nanohardness [54]. Specifically, the use of a fibre laser enables a finer kerf width to be achieved compared to those obtained with Nd:YAG lasers, owing to the higher beam quality. It was also emphasised that the initial microstructure could yield surprising results. The initial average grain size was approximately 50 μm, and, although no recrystallisation was detected, the nanohardness in the melted zone was lower than that in the base material. This result is unusual because heating typically promotes grain growth, as described elsewhere [19]. This finding is of interest because

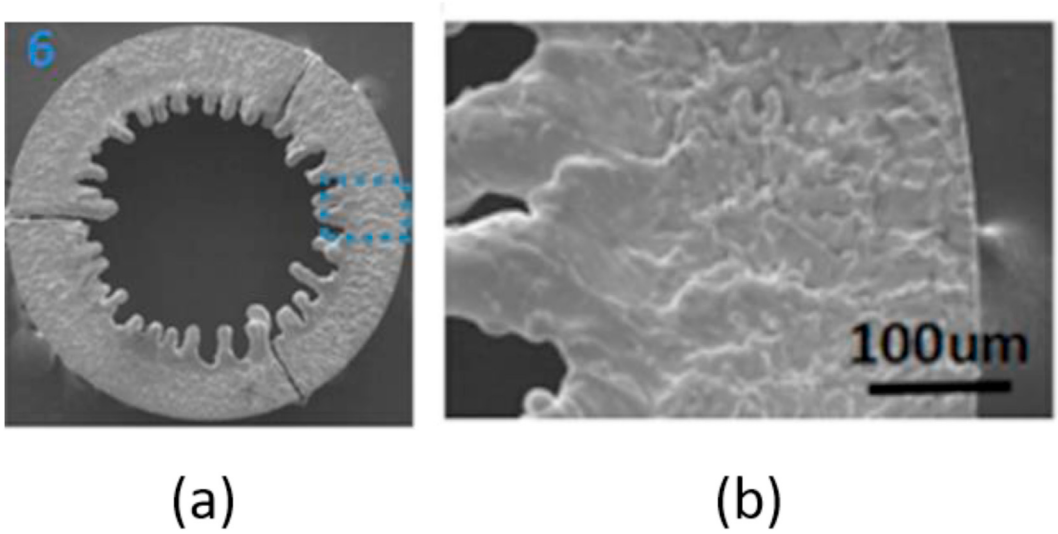


**Fig. 14 – SEM images of NiTi laser cut tube, showing the formation of debris: entire cross section of the laser cut tube (a), and magnification of the melted material zone (b) [56].**

the recrystallisation in NiTi induces variations in the hardness, stress–strain, and strain recovery, as well as modification of the MT in terms of the peak shapes and characteristic temperatures [46].

The effects of different shielding gases, such as Ar and N, and their pressure on kerf formation in laser cutting on thin NiTiCu tapes were investigated using a nanosecond fibre laser [46]. Whereas Ar promoted the formation of a large amount of spatter evenly distributed on the exit surface, N generated more irregular kerf width, numerous small drops of melted material, and a lesser amount of spatter. However, the gas pressure should also be selected considering that bending of the NiTi sheets during cutting must be avoided [49].

The interest of several authors in studying the formation of spatter and recrystallisation layers is due to the industrial requirements of post-processing for finishing surfaces. Finally, it can be concluded that the use of a long or short pulse regime does not offer sufficient quality from the perspective of realising mini- or micro-elements. Momma et al. suggested that the use of common PW laser sources, from old Nd:YAG lasers to the newest active fibre lasers, producing laser pulses from milliseconds to nanoseconds, has some limitations in stent cutting [58]. Since 1999, the adoption of ultrashort lasers has been implemented given the potential to cut nearly every type of material with minimum mechanical and thermal damage.

#### 4.1.2. *Effects of ultrashort laser pulses*

More limited alteration of the kerf surface can be linked to better control of the heat as input of the process, improving the precision of the process and the final performance of the material. Thus, the use of shorter pulse durations has been more intensively addressed in the literature for cutting NiTi SMAs than for the laser processing of other materials [59]. In fact, most studies on NiTi SMA cutting have been based on the use of ultrashort pulsed lasers. Further, to overcome the potential residual overheating during ultrashort laser processing of NiTi SMA, other technological solutions have been researched to perform cutting under liquid for a double benefit. First, this approach enables the drops of melted and vaporised material to be blown away more effectively, allowing higher quality. Second, the cooling of the NiTi parts is considerably improved, further hindering local heating and consequently limiting the HAZ extension.

As described in Section 3.2, ultrashort laser pulses can induce ablation of the material through rapid vaporisation and limit the melted material in the laser–material interaction zone. When the laser pulse stops, the material lattice experiences the influence of the overheated electrons, resulting in high precision and minimal thermal damage [40]. The most evident effect of the negligible heat diffusion can be observed in laser surface modifications; in particular, in laser texturing the modified surfaces are free from any significant drops of melted material and the surface morphology exhibits periodic micro/nano structures. These surfaces can modify largely the wetting properties, and consequently the possibility of controlling the cellular proliferation, very attractive for biomedical devices [60–62].

Anyways, typically regarding the laser cutting process, negligible traces of melted material can be found attached to the back side of the tube, which is a remarkable achievement in laser cutting of medical devices, because the surface quality requirements are very strict.

NiTi thin-walled tubes were laser-cut using an ultraviolet (UV) picosecond laser with a pulse duration of 6 ps, with excellent performance [42], and femtosecond-free cuts with sharp edges were achieved, as depicted in Fig. 15. Even though the process was performed with a pulse duration slightly longer than the threshold for avoiding heat conduction in metals (i.e. 1 ps), the laser-cut thin tubes exhibited thin kerf and the absence of melted material. The average roughness of the laser-cut surface was as low as 1.34 μm, satisfying the high-quality surface requirement for stent manufacturing. A recrystallised zone 10 μm from the external surface was

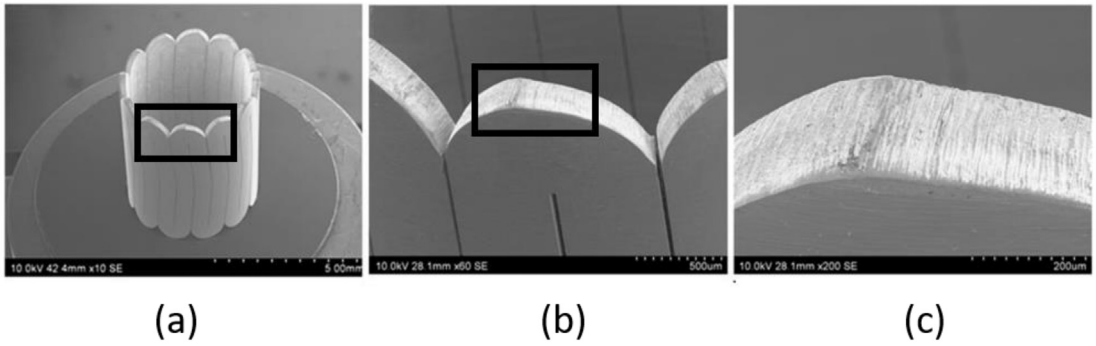


**Fig. 15 – SEM images of the NiTi cut edge obtained with a picosecond laser, at different magnifications [42].**

measured using the nanohardness profile. In addition to the use of the picosecond regime, the adoption of an emission wavelength shorter than that of the infrared field can induce higher absorption and focussing ability, making this laser source well suited for the machining of delicate and thin materials for stent applications. Based on this work, the obtained cutting quality should reduce the post-processing requirements. In fact, the main contribution to the surface roughness is associated with striations, which are generated for hydrodynamic instability of the melted front.

When the pulse duration is reduced to hundreds of femtoseconds, the absorbed energy is firstly transformed into electron thermal energy, and a relevant portion of the latter is transferred to the lattice [63]. Thermal diffusion into the material is minimal, leading to a negligible amount of melted material. Absorption is predominant over thermal diffusivity, and heat conduction can be considered negligible.

In the early works dedicated to the use of femtosecond laser cutting of NiTi SMAs, the average power of the laser sources was limited to the range of hundreds of milliwatts to a few watts, offering very limited productivity rates. For a Gaussian distribution, the ablation diameter can generally be described well by Eq. (2), where F is the fluence, $F_{th}$ is the threshold fluence for material removal, and $D_0$ is the incident diameter of the laser beam, unless air breakdown occurs, as in the case of ultrashort laser machining with high average power [64]:

$$D = D_0 * \sqrt{\frac{1}{2} * \ln\left(\frac{F}{F_{th}}\right)}. \quad (2)$$

This relationship shows that it is possible to machine features smaller than the laser spot size. This ability is explained by the fact that, because the beam distribution is Gaussian, the external layer contains little energy, and this energy can be lower than the threshold for material ablation.

In ultrashort laser processing, the fluence needs to exceed a threshold value, called the ablation threshold fluence ($F_{th}$) to enable ablation; this value depends on the interaction of the laser with the material. Likely the first work published in the literature reported the determination of the threshold values for the processing of NiTi samples in the femtosecond regime, discriminating between gentle and strong ablation conditions [65]. This threshold fluence value was evaluated experimentally (see Fig. 16), as shown in the graph of the measured ablated diameter ($D^2$) versus the applied fluence ($F_i$). A semi-log plot was obtained, and a linear curve was fitted to the data. The ablation threshold fluence was then evaluated from this

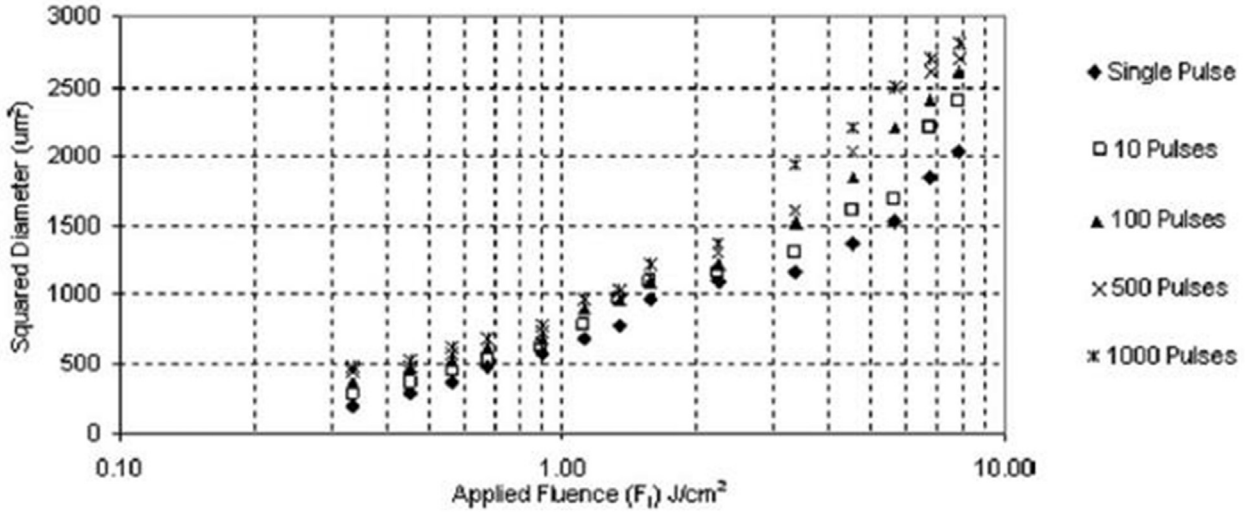


**Fig. 16 – Single- and multi-shot ablation threshold fluences for Nitinol [65].**

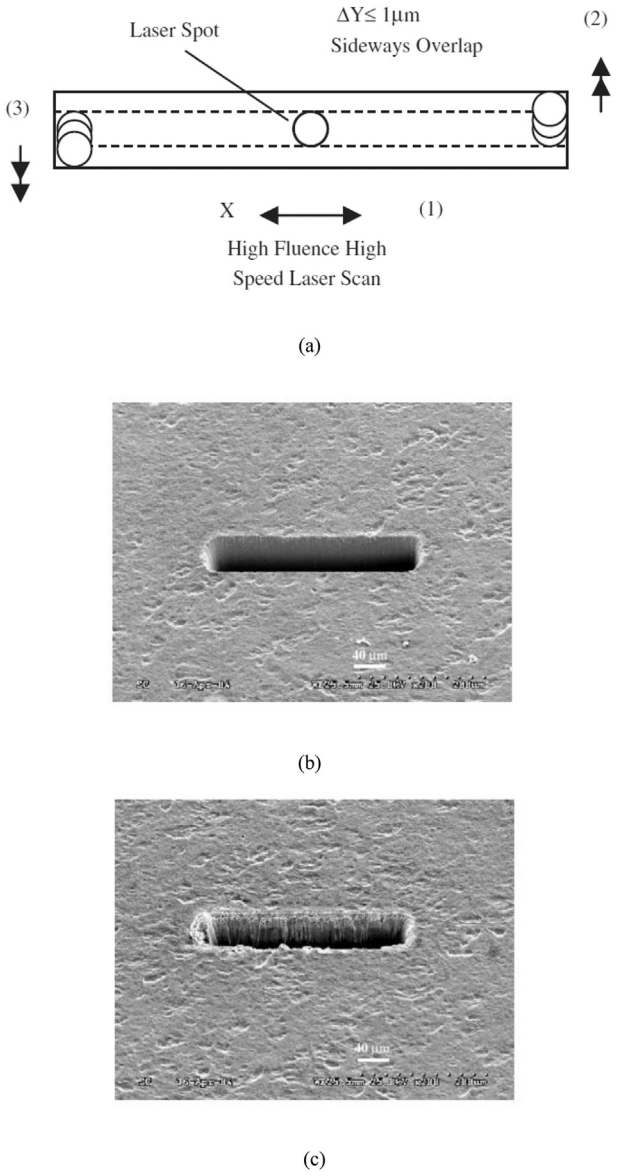


**Fig. 17 – Sideways-movement path to eliminate recast material and minimise the HAZ for high-throughput femtosecond laser cutting at a high fluence of NiTi (a) and laser cut kerf obtained with the sideways-movement (b) and conventional paths (c) [64].**

plot by extrapolating the linear fit to the intersection with the abscissa, that is, when $D^2 = 0$. After the applied fluence is increased to a certain level, the slope changes, which means that two regions with different ablation processes can be distinguished: gentle and strong ablation. The gentle process is characterised by low material removal, which occurs via vaporisation, whereas the strong process is characterised by a rougher surface because of the phase explosion. Gentle ablation is ideal for features with very high-precision requirements. The threshold fluence for ablation should be calculated in both situations, as previously explained.

The threshold fluence also decreases with increasing number of pulses, because more energy is introduced into the material, even though Nitinol does not present strong heat accumulation (see Fig. 16). This behaviour is mainly linked to the incubation effect, which is attributed to the interaction of multiple pulses with fluences lower than the single-shot ablation threshold fluence, which can cause surface defects and could lead to ablation below the single-pulse threshold value. Nitinol can exhibit a weak accumulation effect compared with other metals due to its high incubation coefficient (0.95). This characteristic indicates that Nitinol experiences low heat accumulation, offering some benefits: an increase in the material removal rate and the achievement of dimensional accuracy and high surface quality.

In another work, Quintino et al. reported some empirical equations for determining the width and depth of cutting using a 2 W average power. Specifically, the surfaces processed with a low cutting speed (0.01 mm/s) exhibited the presence of resolidified thin layers with cracks and oxides; increasing the cutting speed up to 1 mm/s provoked an improvement in the surface quality, owing to the shorter interaction time [66]. Moreover, Ni depletion was observed, which could be beneficial for biomedical devices. The effects of some process parameters, such as focal position and laser power, on the kerf width were analysed [66]. Cutting edges with aspect ratios as high as 60 were produced with nearly vertical sidewalls. However, suitable selection of the process parameters permits the avoidance of Ni vaporisation, leaving the chemical composition of the alloy unchanged [67]. In addition, a homogeneous surface morphology was detected, facilitating post-processing and coating for different purposes.

Another important parameter is the laser scanning path, which indicates the motion strategy of the laser beam during the cutting process. Li et al. proposed a particular laser path, namely, the sideways-movement path, to balance the trade-off between the surface quality of the laser cut kerf and the productivity rate [64]. In particular, at a low fluence, the penetration depth is quite limited; this characteristic improves the cutting properties but can greatly reduce the production capacity of the system. High productivity and high precision can be balanced by implementing a path-planning technique, whose principle is shown in Fig. 17. A first high-power scan is performed, followed by two sideways scans moving 1 μm to the left and then to the right, at a fluence just above the ablation threshold in order to improve the quality.

Other types of cutting paths, depicted in Fig. 18, were investigated directly on the curved surfaces of thin-walled NiTi tubes in two studies [35,68]. In the first work, the energy accumulation was accounted for to explain the selection of the best scanning strategy in terms of surface quality [68]. In the second study, the authors investigated the potential of cutting sharp edges for stent manufacturing. In particular, the squared edges of the stent could be directly processed to rounded edges from steep and square edges without any sign of HAZ [35]. Thus, using round stent edges enhanced the radius considerably, which not only removed the square and steep edges, but also produced no side effects after the femtosecond laser scanning process with a programmed laser movement path. The rounded edges of the stent retained its original surface features, enabling the avoidance of post-processing, such as chemical etching, in which the stent edges are rounded after femtosecond laser micromachining via a cleaning process.

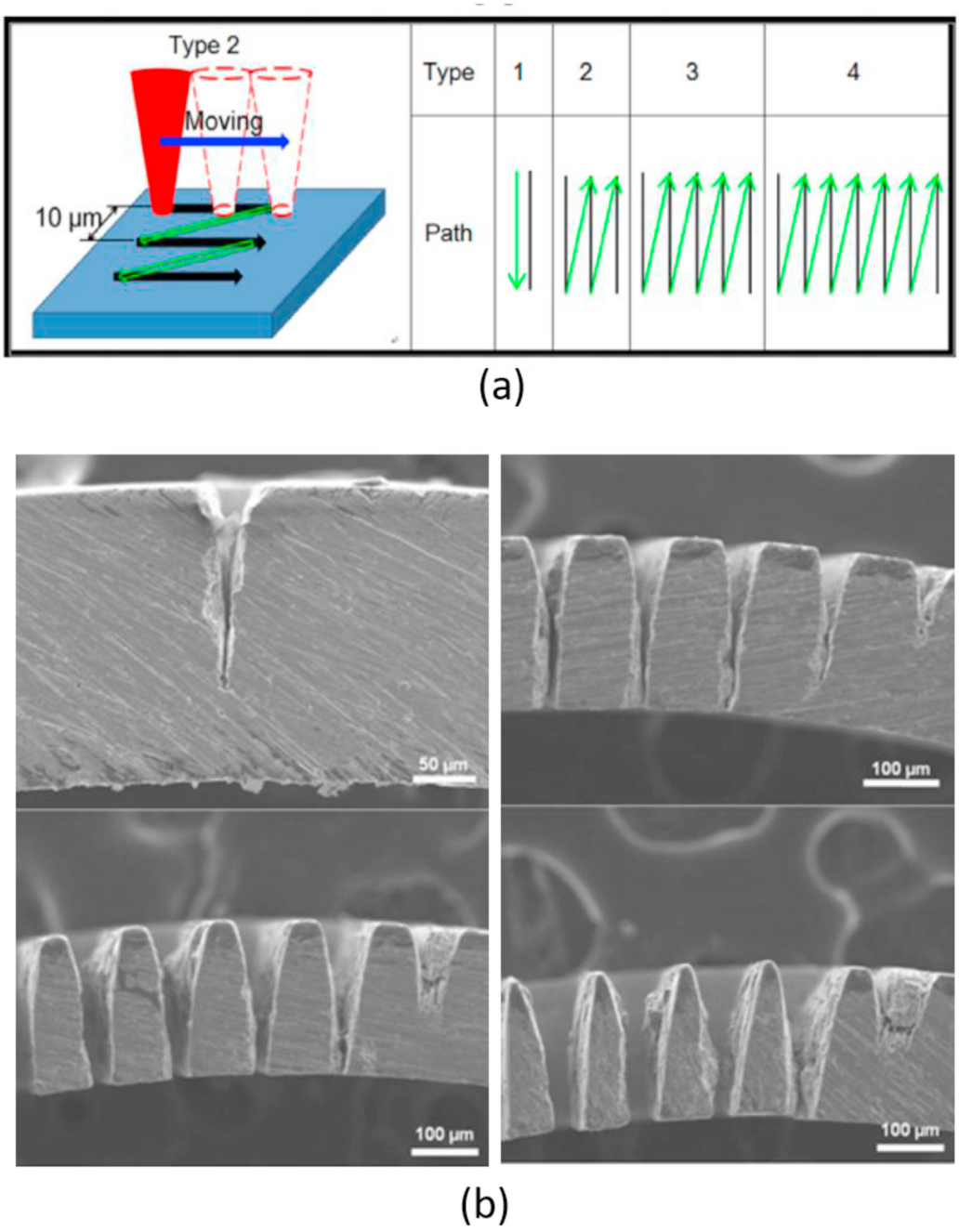


**Fig. 18 – Schematic of the investigated laser scanning paths (a) and corresponding cross-sections of the NiTi laser cut kerf (b) [35,68].**

Because of this promising performance in the femtosecond laser processing of NiTi SMA, Huang et al. compared the surface quality resulting from femtosecond cutting and wire electrical discharge machining (WEDM) [69]. Femtosecond laser cutting enabled the kerf width to be finer than that achievable via WEDM, and the surface quality was higher in terms of Ra. On the contrary, low-average-power femtosecond lasers offer significantly lower material removal rates than WEDM.

Recently, the development of high-power femtosecond lasers has enabled the achievement of maximum average power values as high as some tenths of watts, making the process faster and more reliable for industrial purposes.

#### 4.1.3. *Technological solutions for improving cooling during laser cutting*

The decrease in pulse duration from the millisecond to nanosecond regime does not drastically change the formation of melted material, and significant microstructural alteration can be observed. Further decreasing the pulse duration down to the femtosecond regime can clarify the improvements in surface quality, negligible thermal modifications, and dimensional

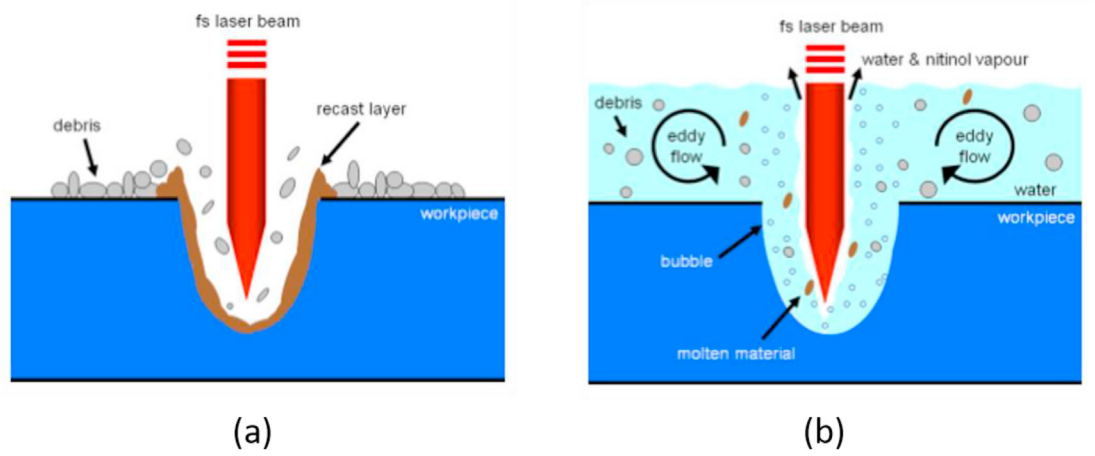


**Fig. 19 – Schematic of interaction between femtosecond laser pulse and material in dry (a) and underwater (b) process [70].**

accuracy. However, ultrashort laser processing may not be sufficient to preserve the functional performance of the microdevice. Therefore, various technological solutions have been proposed to overcome these issues.

(i) Liquid-assisted laser processing [70];
(ii) Water-jet guided laser beam machining [71];
(iii) Changing the type of laser–matter interaction involved during laser ablation by reducing the emission wavelength in the UV field [72].

The first approach regards the realisation of femtosecond laser cutting of thin-walled tubes immersed in a thin layer of water [70]. The main achievements associated with the use of the liquid are the absence of an HAZ, debris, spatter, and recast material and fine kerf quality, whereas the dry process yields comparable surface quality and the presence of recast material, owing to the previous vaporisation and consequent resolidification in situ.

In fact, during dry ultrashort laser cutting, negligible melting occurs and the material is suddenly vaporised owing to the large power densities, on the order of megawatts per centimetre, reached during the process. Thus, the area around the cut affected by the process is quite thin, hence the modification of the material properties (see the schematic in Fig. 19a).

To achieve faster cooling, the technological solution proposed by Muhammad et al. suggests changing the environment in which laser cutting is performed. The laser beam can irradiate the material, which is placed under a liquid film such as water (see the schematic in Fig. 19b). The main benefit is associated with a softening effect of the thermal cycle intensity reached near the kerf, minimising the heat conduction and limiting the thermally affected material.

Dry femtosecond cutting resulted in the absence of an HAZ but the presence of debris and recast material, caused by the in situ solidification of the vaporised material (see Fig. 20a). In contrast, in water-assisted femtosecond laser cutting, no HAZ, debris, or recast material were present and high kerf quality was detected (see Fig. 20b). The dual benefit of the water was described as resulting from cooling through the convection and generation of bubbles, which facilitated debris removal. Water convection can change the temperature field during the process, and the authors reported that submerged cutting requires higher fluence and lower cutting speed, whereas dry cutting requires opposite values of the main process parameters. Moreover, the generation of bubbles can improve the removal of residual debris, producing surface quality similar to that after ultrasonic cleaning. It can be concluded that water can increase the benefits associated with shielding gas, which is commonly used in conventional laser cutting.

Another innovative method for precise cutting by creating a cooling environment is the so-called water jet guided laser beam machining (WJGLBM) approach, which was presented and patented by Synova [73]. This innovative technology works with a particular method for laser beam delivery, based on the principle of total internal reflection of the laser beam inside a low-pressure water jet. Fig. 21a shows a schematic of WJGLBM [71]. The laser no longer has a Gaussian distribution; instead, its shape becomes constant and depends only on the coherence of the water jet. Laser processing utilises a focused laser beam and the strong cooling capability associated with the water flowing on the irradiated surface. Specifically, the PW laser emission mode ensures continuous alternation between heating during laser pulses and cooling between laser pulses, induced by the water flow. In this case, the surface quality can be dramatically improved with respect to that in dry laser cutting, as depicted in Fig. 21b. The absence of mechanical and thermal damages provokes the generation of cracks in the cutting kerf, and no microstructural changes occur in the material. The water jet presents very high levels of kinetic energy owing to the high initial pressure, which increases the efficiency of material removal and creates less burr and recasts. Moreover, the water can cool the surface surrounding the cut, producing a cut with almost no HAZ or defects, which is fundamental in micro-devices.

Finally, the third solution utilises UV lasers, which can limit the thermal input and increase the process precision, owing to the small laser spot size. Despite these benefits, this process is usually unsuitable for the machining of metals

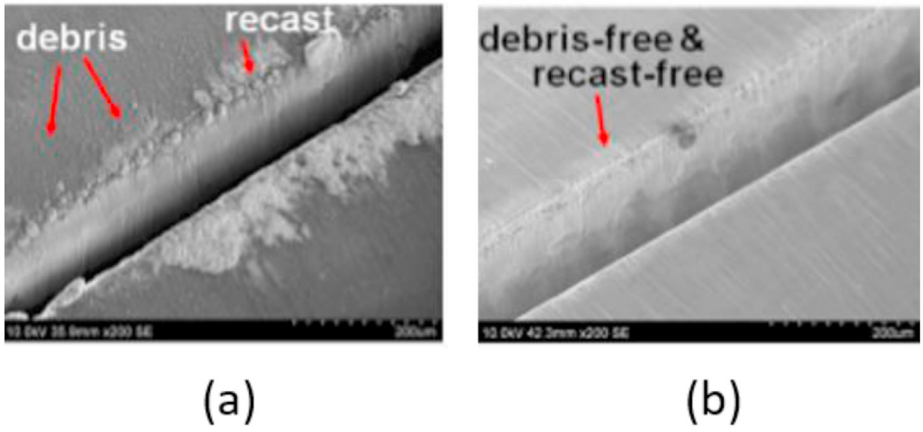


**Fig. 20 – Kerf quality obtained through (a) dry and (b) underwater laser cutting of NiTi tubes [70].**

because of the type of interaction with the material, which involves acting directly at the atomic bond level, and because of the very low productivity obtained. Therefore, very few studies have been conducted on the use of UV lasers in the laser cutting of Nitinol. Yung et al. investigated the effects of different process parameters, such as pulse energy, scanning speed, repetition rate, number of laser passes, and laser beam size, on kerf quality in laser cutting performed with a 355 nm emission wavelength [72]. Under the optimal process conditions, the kerf was as thin as 25 μm and exhibited very limited taper, equal to 1° at a thickness of 350 μm. Moreover, no HAZ was observed. Hundreds of laser passes were required for complete realisation through the cutting edge, because low power was irradiated in each pass. However, this technological solution provides limited productivity for metal cutting. Therefore, it can be considered less promising than the previous two solutions for improving cutting performance without reducing productivity.

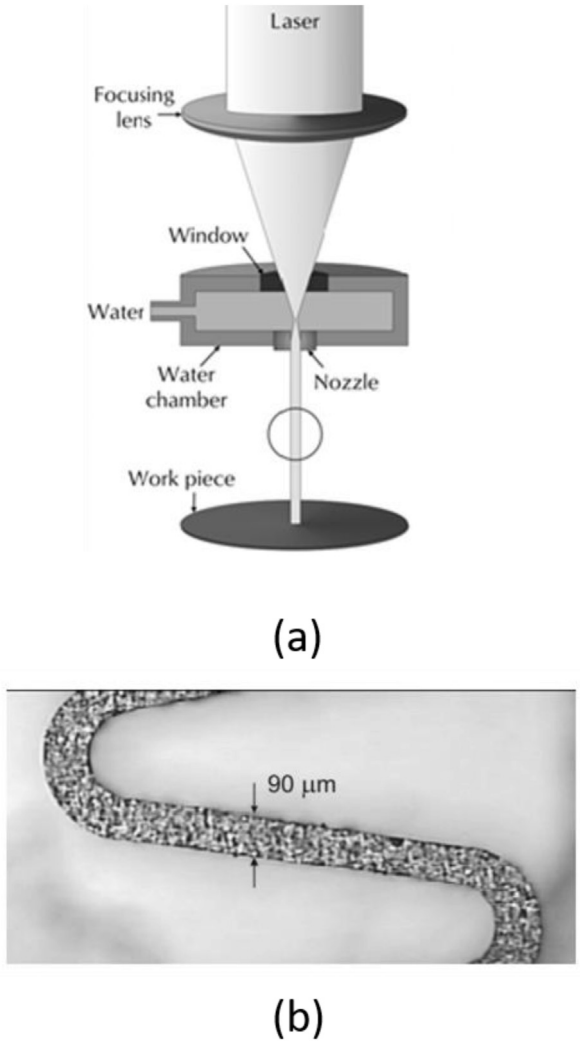


**Fig. 21 – Schematic of the WJGLBM process (a) and optical microscopy image of the back side of a Nitinol stent (b) [71].**

### 4.2. *Thermal modelling*

The laser cutting process is very complex, but estimation of the temperature field is a fundamental aspect. Heating occurs during laser beam irradiation, whereas during cooling, two energy loss mechanisms should be considered [49]. First, radiation loss can be correlated with the visible plasma plume localised within the cutting kerf, which causes prolonged post-pulse heating and therefore produces undesired additional melt formation, increasing the kerf width. Second, heat conduction can cause a temperature increase within the material, heat the surrounding material, and cool the irradiated volume. The analytical temperature profile could not be determined for this complex process. The temperature change of the surface can be estimated from a simplified model related to the pulse duration, t, and intensity, I, according to Eq. (3):

$$\Delta T_{surf} \propto I\sqrt{t}. \tag{3}$$

This equation leads to the concept that short laser pulses result in a small zone being heated to high temperatures and to a narrow temperature distribution with a high peak level induced within the material. These characteristics enable the achievement of high temperatures in the liquid melt pool, making it easy to blow out. However, owing to the complexity

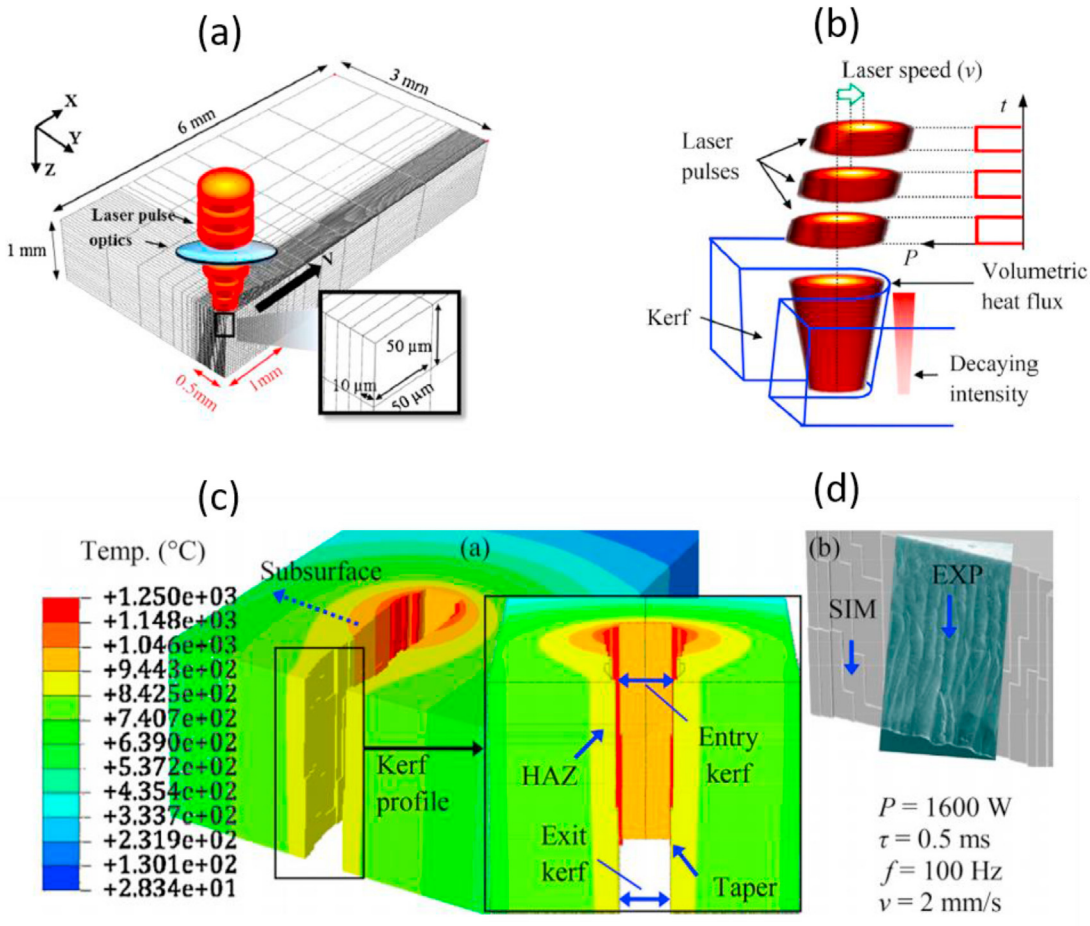


**Fig. 22 – Simulation schematic of pulsed laser cutting (a) and the moving volumetric heat flux of a pulsed laser (b); prediction of the laser cut kerf (c) and comparison between numerical and experimental striations placed on the lateral view of the kerf during NiTi laser cutting (d) [74].**

of the laser cutting process, analytical solutions can be exceeded, making numerical modelling more precise and accurate in temperature field determination.

By implementing a thermo-mechanical model of NiTi SMA, it is possible to study the process to optimise the parameters, producing excellent results with few thermal defects and limited HAZ. It is well known that the laser cutting process can induce a complex temperature field, stress distribution, and, consequently, HAZ formation, which are critical aspects of the integrity of laser-cut NiTi parts. However, these features are difficult to measure experimentally owing to their rapid transient process. To clarify the process mechanics in laser cutting of NiTi SMA, Fu et al. developed a 3D finite element model (FEM) of PW laser cutting [74,75].

A typical heat flux source model has the following form:

$$I = \frac{AP}{\pi r_0^2} \exp\left[ - B\left(\frac{r}{r_0}\right)^2 \right], \tag{4}$$

where I is the laser intensity, A is the laser absorption coefficient, P is the laser power, $r_0$ is the spot radius, B is the shape factor of the Gaussian distributed heat flux, and r is the distance to the beam centre. This form was selected it because can offer the best matches with the experimental results.

A novel moving volumetric pulsed heat flux model was proposed, and a specific material subroutine was incorporated to model SE and the SME. The 3D heat source model consists of a moving conical shape volumetric heat flux, the shape of which is depicted in Fig. 22a and b, with a pulse shape assumed to be perfectly rectangular.

A subroutine was dedicated to definition of the 3D heat flux source, according to the following characteristics: (i) moving Gaussian heat flux from the laser beam, (ii) a PW emission mode, and (iii) conical volumetric heat flux. The kerf width was predicted and validated under different process conditions to ensure consistency with the numerical results. The actual form of the 3D heat flux model used in these studies is as follows:

$$F = \frac{CP}{\pi R_0^2 h} e^{\left(-3\left(x^2+y^2\right)/r^2\right)} \theta(f, \tau), \tag{5}$$

where F is the applied heat flux, C is the energy absorption coefficient, P is the peak pulse power, $R_0$ is the laser spot radius on the top surface, h is the sample thickness, f is the laser frequency, $\tau$ is the pulse width, and r is the instantaneous radius of the heat flux, which is characterised by a conical shape. The 2D cartesian coordinate system is expressed by x and y, respectively.

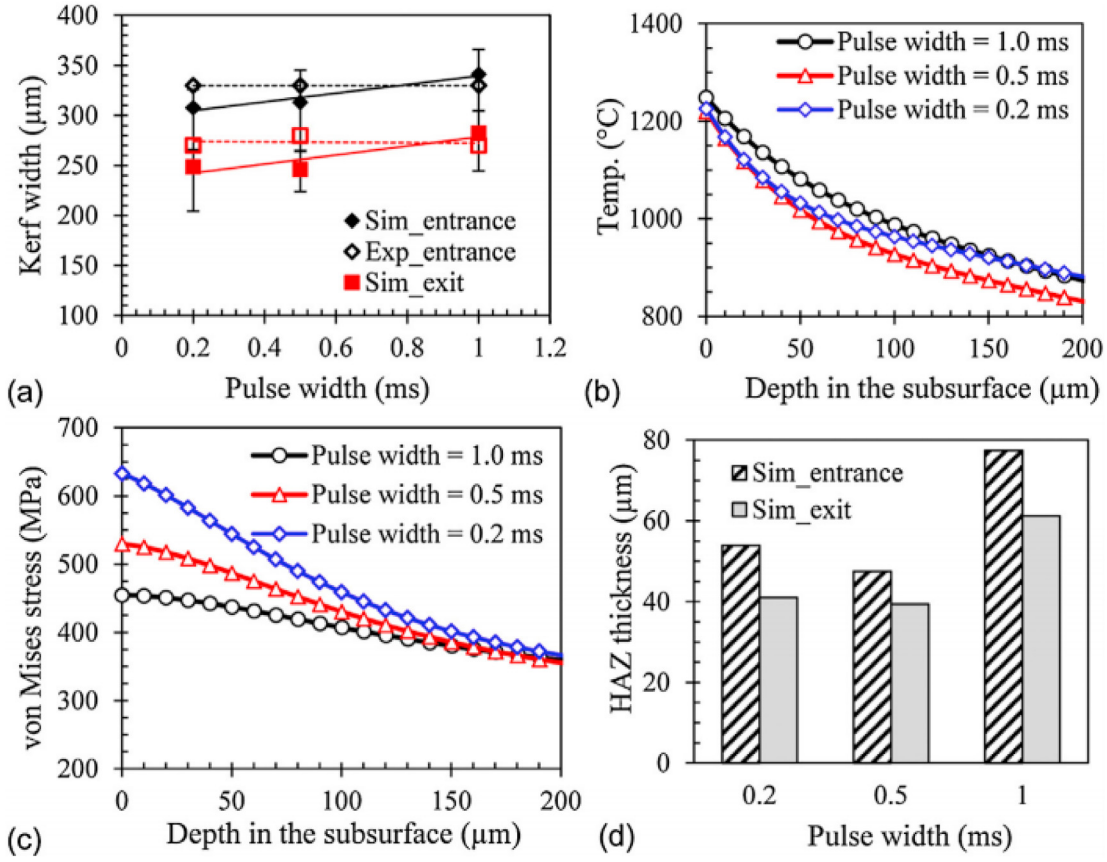


**Fig. 23 – (a) Kerf width, (b) temperature, (c) stress, and (d) HAZ size estimated as functions of the pulse width [75].**

Fig. 22c and d show the kerf shape determined with the transient temperature contour. The mesh elements with temperatures higher than the melting point were removed from the mesh, highlighting the kerf formation. The assumption underlying this is that all the melted material can be completely removed. From the FEM results, other kerf characteristics, such as taper, striations, and HAZ extension, were also calculated. The temperature field was also evaluated to determine the stress distribution, and it was found that the highest stress (520 MPa) was associated with slow motion of the laser beam, due to intense heat conduction into the workpiece. In contrast, it was determined that high peak powers can maximise the stress near the upper surface, whereas low peak powers increase the stress below the upper surface.

Fig. 23 depicts a representative set of variables, which were determined using the presented FEM. This approach is very promising for supporting feasibility area identification, which is typically conducted experimentally and for elucidating the complex phenomena associated with PW laser cutting of NiTi SMA.

### 4.3. *Microstructural and functional characterizations*

For typical NiTi devices, such as stents and actuators, the microstructure must be carefully controlled to ensure that the mechanical response and biocompatibility are maintained. The specific operating conditions of laser cutting can affect both the microstructure and the corresponding functional performance of NiTi parts. In fact, laser cutting is a thermal process, and some heat generated by the laser is transferred to the material surrounding the cut zone, which can modify it, producing recrystallisation and, thus, a change in microstructure, which can deteriorate the characteristic properties of the material. Thermal diffusion is directly proportional to the interaction time between the laser and material. Therefore, the shorter the pulse duration, the more limited the HAZ.

#### 4.3.1. *Microstructure*

CW lasers, or PW lasers operating in the long-pulse-duration regime, work mainly in the liquid phase, and a large amount of heat is transferred to the material, causing recrystallisation and significant microstructural variation. The use of a Nd:YAG laser in the cutting process can promote the formation of a recast layer of approximately 30 μm [76] and microcracks, owing to the rapid cooling rate [77].

Fig. 24 shows the microstructural changes observed at low magnifications by optical microscopy [53]. Near the kerf side, the grain size was significantly enlarged with respect to the base material. The HAZ exhibited a microstructural gradient depending on the temperature level experienced by the material during laser cutting. This finding suggests that the cutting of thin parts using CW or long-pulse-duration lasers can promote a complete change in the microstructure, making it

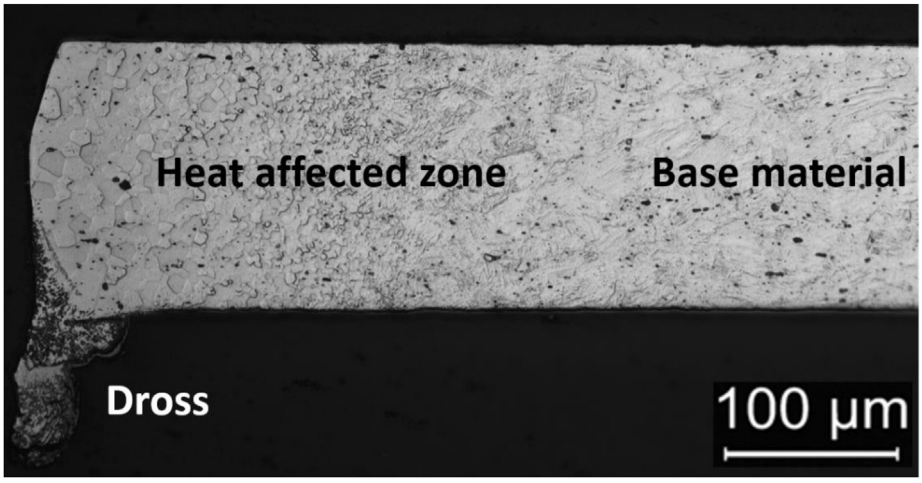


**Fig. 24 – Microstructural evolution from the kerf side (left) to the base material (right), correlated with the use of a CW fibre laser in NiTi tape cutting [53].**

impossible to use any post-processing to recover the initial microstructure.

This property change becomes particularly critical in the case of microdevices, in which the small dimensions of the components increase the importance to the modifications generated by the laser cutting process, which should then be reduced or removed with the subsequent post-processing. Post-processing results are critical for small components because the removal of the associated material may be too large with respect to the component thickness.

Toro et al. investigated the microstructure evolution, analysed with high resolution via transmission electron microscopy (TEM), promoted by laser cutting of cold-worked NiTi tubes for stent production [77]. The recast layer exhibited recrystallised, almost equiaxed grains of parent-phase B2, whereas the base material in cold-worked conditions exhibited a cubic parent phase and monoclinic martensite B19′. Fig. 25 shows the microstructure variation. Rapid cooling, induced by the laser cutting process, removed the dislocations and strains present in the B2 matrix, and grain growth was achieved.

#### 4.3.2. *Functional behaviour*

Such intense effects of laser cutting, performed using long pulses, can promote considerable variation in the MT operating temperature, which is associated with microstructural modifications. Tuissi et al. investigated the shift in the MT of superelastic NiTi processed using a CW fibre laser. The presence of intense and sharp MT peaks suggests that the material was subjected to strong overheating during cutting, which can be correlated with large thermal diffusion [78]. This effect can drastically change the functional performance of the NiTi element, and its effect on the material properties can be linked to equivalent high-temperature heat treatment involving solubilisation [79,80]. A high-performance shape memory effect (HPSME) was observed in diamond-like elements, as shown in Fig. 26. Extremely high elongation values (with a stroke of approximately 30% of the diamond length) were recovered under an applied force of 0.7 N within a temperature range of 50 °C.

In good agreement with the reported results obtained using the technological approach, the adoption of short laser pulses in the nanosecond regime did not significantly limit the modification of the functional properties of the NiTi elements. Nespoli et al. reported the functional properties of a snake-like element, which was laser-cut from thin SMA NiTi tape (0.12 mm in thickness) with a nanosecond fibre laser [81]. Owing to the formation of recast material during processing, two post-processing steps were also taken into account to finish the surfaces. Fig. 27 shows the evolution of the surfaces of the snake-like element under different conditions: with laser cutting, after simple pickling, and after pickling and electro-polishing. As the laser-cut surface exhibited a significant amount of melted material, pickling could remove most of the recast layer from both surfaces, whereas electropolishing primarily affected the surface finish. In fact, the removal of the laser-affected material was correlated with an MT shift observed by differential scanning calorimetry (DSC) analysis, as shown in Fig. 27g. As the DSC scan of the initial sheet indicated that MT was associated with a double transformation with wide peaks, the laser-cut sample exhibited sharper peaks with changes in the characteristic temperatures. These results are comparable to those obtained by Tuissi et al. [78]. After the two steps of post-processing, the shapes of the peaks and the corresponding MT operating temperatures tended to shift toward those of the base material [31,81,82]. Similar results were achieved even for reverse MT upon heating. Strain recovery testing of the samples under different conditions yielded results attributable to the DSC measurements. The snake-like element in the laser-cut condition exhibited an almost negligible displacement induced by the temperature change, owing to the overheating of the alloy. In contrast, pickling and electropolishing can induce better functional performance, with higher displacements, because of the recovery of the initial MT (see Fig. 27h).

Stabilisation of the functional behaviours of the NiTi elements was achieved after pickling, as also demonstrated by Biffi et al. [82,83]. Fig. 28 shows the strain recovery under a constant load upon thermal cycling of chemically etched

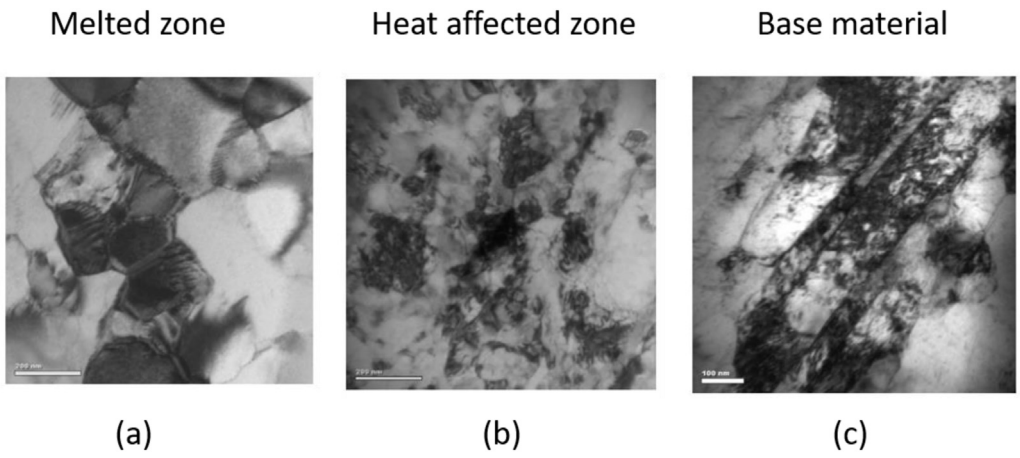


**Fig. 25 – TEM images of NiTi in the (a) recast layer, (b) HAZ, and base material (c) [77].**

snake-like elements in NiTi SMA and the corresponding evolution of the stroke versus the number of cycles. The removal of recast material through chemical etching enabled the elimination of harder material, which is typically induced by rapid solidification. This process enabled the stroke to be increased and the accumulation of plastic deformation to be minimised. Similar results on laser cut surface polishing were achieved after pickling also by other authors [84].

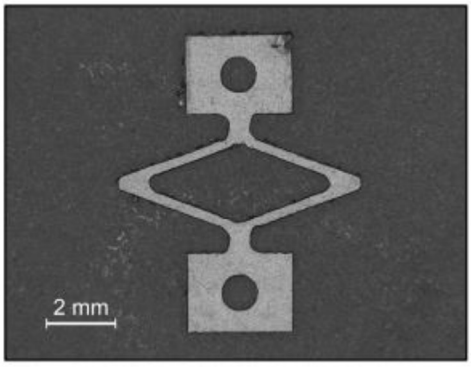


(a)

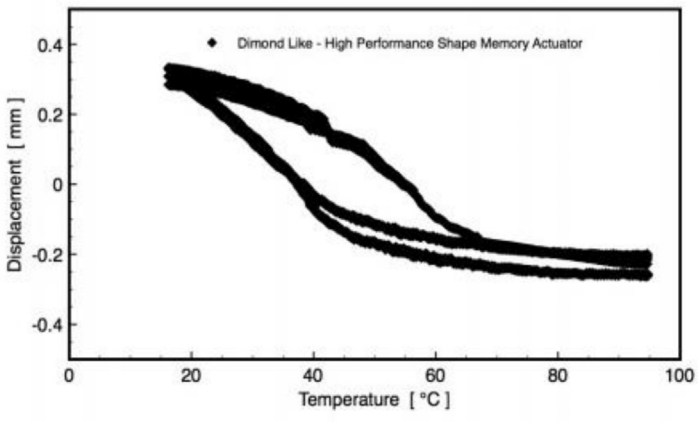


(b)

**Fig. 26 – (a) Laser-machined NiTi diamond-like element and (b) thermal loop under constant load, associated with the HPSME [78].**

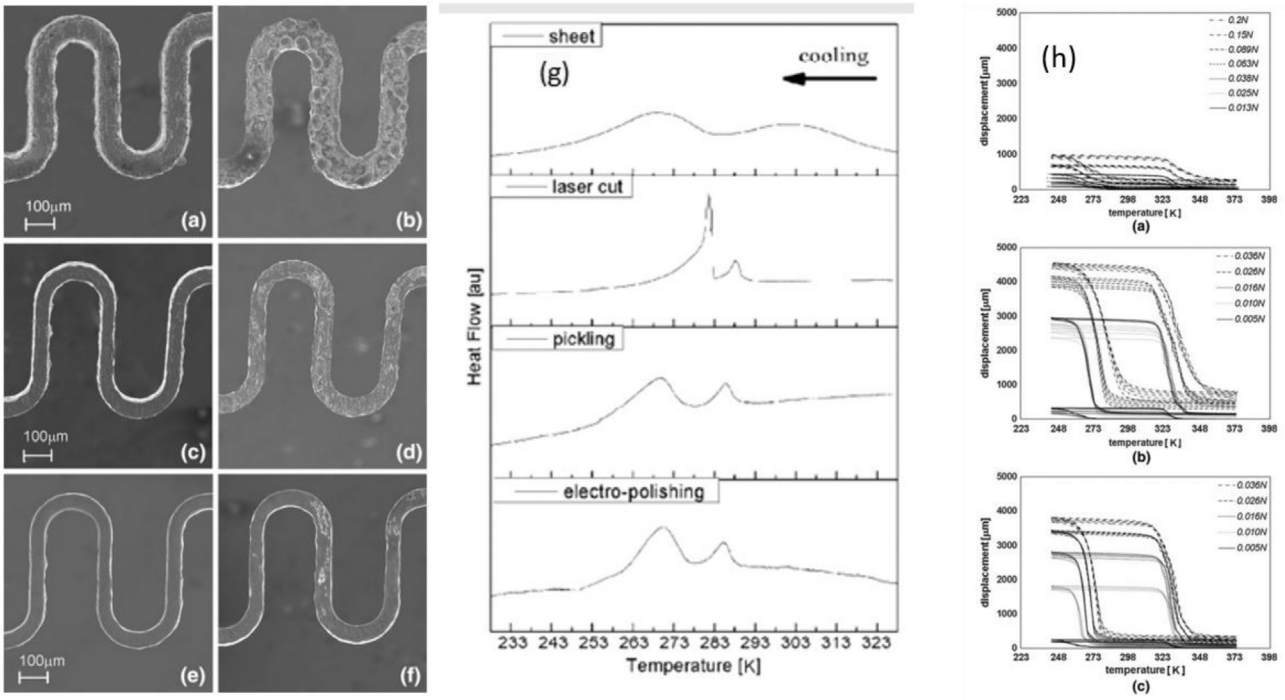


**Fig. 27 – SEM images of the entrance and exit surfaces of the NiTi snake like element: (a) and (b) with laser cutting, (c) and (d) after simple pickling, and (e) and (f) after pickling and electro-polishing, respectively. (g) DSC scan results obtained upon cooling and (h) strain recovery test results of the snake-like elements [81].**

The increase in local hardness was identified using nanohardness profiles. Biffi et al. investigated the effects of different energy densities, obtained by combining different cutting speeds and numbers of laser passes, on the HAZ extension and functional properties of NiTiCu SMA [85]. After nanosecond laser cutting, the ternary SMA exhibited the formation of a multi-stage MT, probably due to the formation of a complex microstructure. The recast material achieved a high nanohardness of 700 HV (versus approximately 200 HV in the base material), and the extension of the corresponding HAZ was on the order of 20–40 μm.

A further decrease in the pulse duration down to the ultrashort regime enabled the thermal diffusion to contract, leaving an almost unvaried microstructure and enhancing the functional performance. Biffi et al. compared the performances of CW and femtosecond regimes in the laser cutting of superelastic NiTi, under straight annealing conditions, on the SMA properties [53]. Because a CW laser generates a large HAZ, it was expected that the material properties could be completely modified. In the case of femtosecond laser cutting, HAZ reduction occurs due to the negligible thermal diffusion associated with the process. Fig. 29 shows the shift of the MT, associated with the use of the CW and femtosecond regimes, from the base material.

With CW laser cutting, the transformation temperatures of the material and enthalpy of transformation are completely

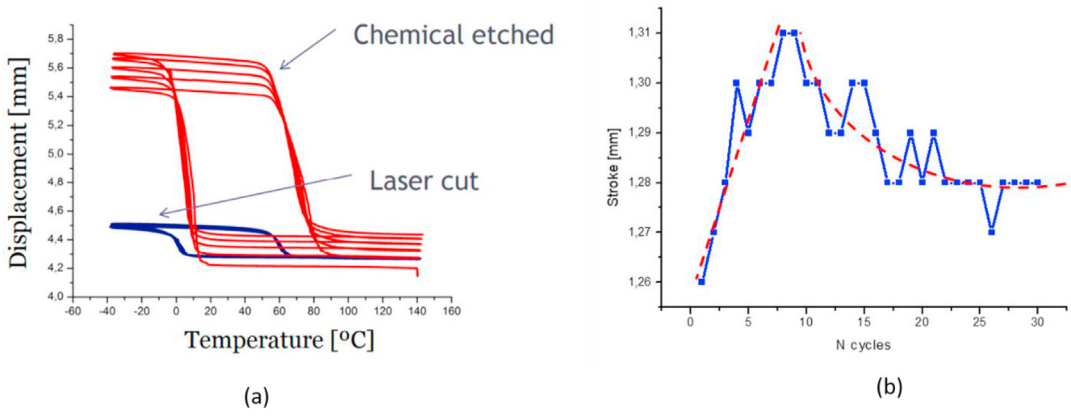


**Fig. 28 – (a) Effects of thermal cycling on the strain recovery of chemically etched snake-like elements in NiTi and (b) stroke evolution [83].**

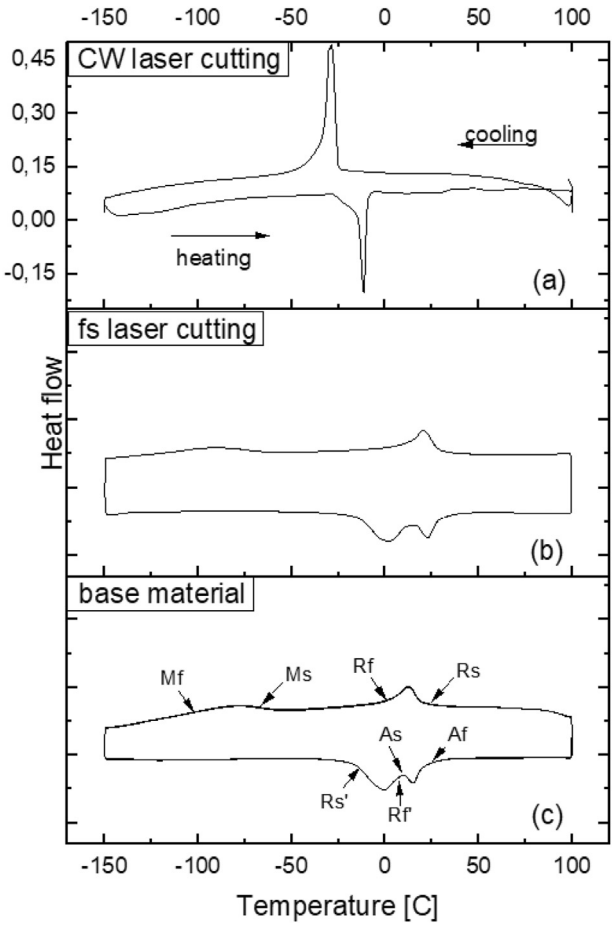


**Fig. 29 – DSC scans of Nitinol machined in the CW (a) and femtosecond regime (b) as well as that of the base material (c).**

modified. In particular, the intense and sharp peaks can be correlated with high-temperature heat-treated NiTi [78]. In the case of femtosecond laser cutting, the peaks remain fundamentally the same in shape and only slightly shift to higher temperatures. In addition, after CW laser processing, the two-step MT becomes a single-step transformation. The superelastic behaviour of the laser-cut element, realised using the femtosecond regime, shows a good superelastic flag-like curve, in which a complete displacement of 2 mm was completely recovered without any residual deformation (see Fig. 30). This behaviour represents the typical superelastic behaviour of commercially available materials [86]. In contrast, this functional behaviour can be considered to be degraded in NiTi elements laser-cut under the CW regime, because the temperature experienced by the material during cutting is higher than that required for inducing SE.

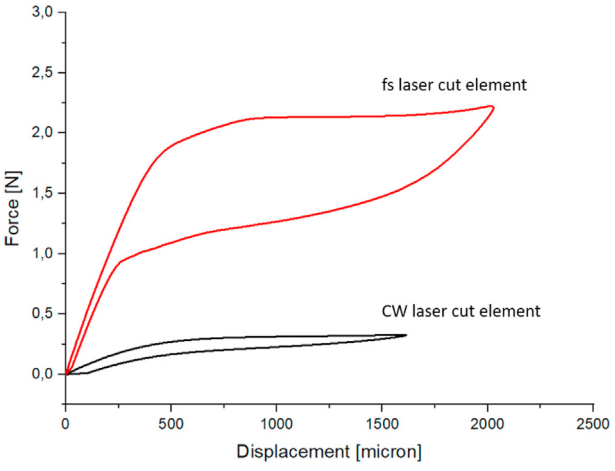


**Fig. 30 – Force–displacement curves of NiTi diamond-like microelements, machined in the CW and femtosecond regime.**

The same authors also investigated the cutting of cold-worked superelastic NiTi tapes in the femtosecond regime [87]. In this case, the only difference between cutting straight-annealed and cold-worked NiTi plates was related to the planarity of the sheet, which could induce larger sensibility in the focus positioning. From an energetic perspective, no differences were observed as the energy required to vaporise the alloy remained the same. It was found that the quality and precision level fully overlapped with those obtained by femtosecond laser cutting of straight-annealed NiTi. In addition, no significant variation in the functional behaviour of cold-worked NiTi was induced by laser cutting, and calorimetric analysis revealed that the flat signal of the DSC scan from the cold-worked material was also observed in the laser-cut samples. In addition, mechanical testing performed at different temperatures indicated that the displacement was almost negligible. This finding confirms that ultrashort laser cutting can be performed to achieve high quality and precision as well as negligible thermal modification of the material properties.

#### 4.3.3. *Corrosion*

Nitinol presents extraordinary corrosion resistance and biocompatibility; therefore, it is one of the most common materials employed in biomedicine. The high-temperature thermal treatment of Nitinol optimises its shape memory properties and generates a layer of oxides on the surface, improving the surface chemistry and biocompatibility.

Owing to the presence of an allergenic element such as Ni, the implementation of devices composed of this material is critical, requiring the adoption of passivation techniques such as electropolishing, which reduces the release of Ni ions [17]. The parameter to be controlled during electropolishing is the amount of material removed during treatment: with more removal, the breakdown potential increases; hence, the corrosion resistance. The more material removed, the thicker the oxide layer formed, and consequently, the more Ni ions released, due to the generation of more constant and Ni-free layer. The stability of this layer was crucial. By removing more material, the oxide layer was reduced.

Decker et al. investigated the corrosion of laser-cut and wire-formed stents. Their results indicated that the amount of material removal in the final surface treatment step (i.e. electropolishing) influences the corrosion resistance for both types of stents [88]. For a more systematic experimental approach, the removal amount was adjusted to create groups with material removal of up to 5%, 5%–10%, and 10%–25%.

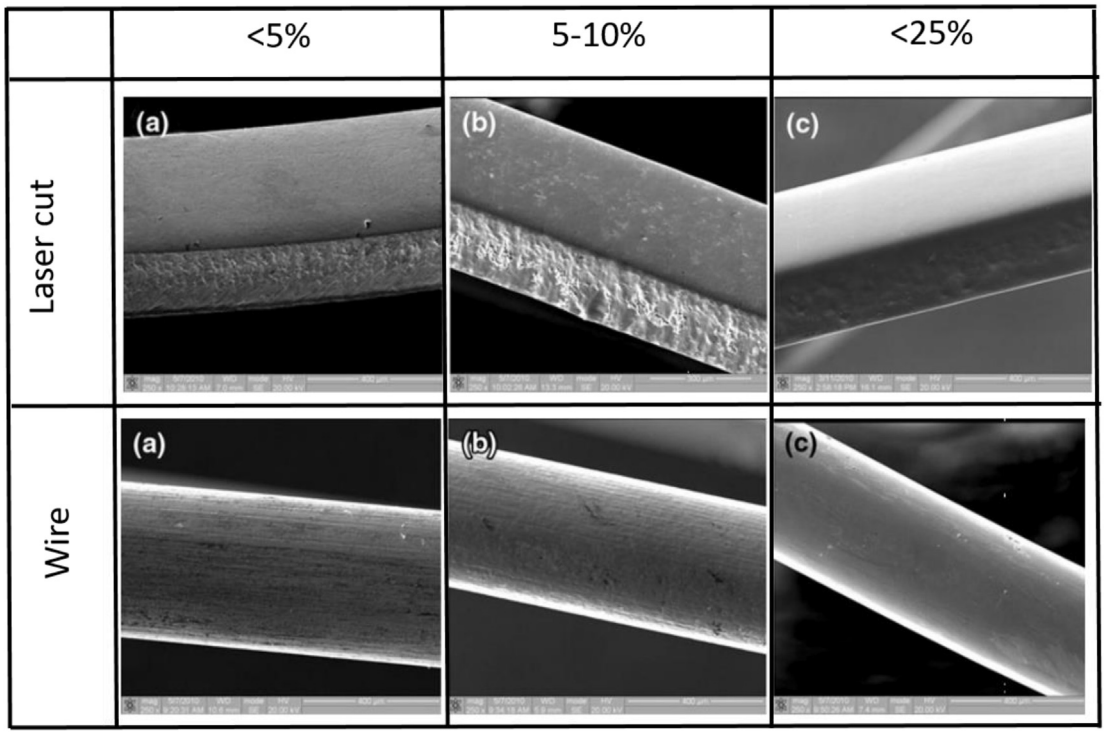


**Fig. 31 – Evolution of the NiTi laser-cut and wire-formed stents subjected to three levels of material removal: (a) below 5%, (b) below 10%, and (c) below 25% [88].**

Fig. 31 show the surface morphology evolution with different material removal levels in electropolishing for laser-cut and wire-formed stents, respectively. It is evident that the main purpose of material removal in post-processing is mainly to finish the laser-cut surfaces, mainly the lateral one where most of the recast material can be placed. Little variation in the surface roughness was observed on the wire surfaces.

Both stent types showed an increase in the corrosion potential breakdown and a decrease in the standard deviation with increasing amount of material removal. Fig. 32 shows the variation of the potential versus the amount of material removal of the laser-cut and wire-formed stents.

It was found that laser cutting requires more material removal to achieve the corrosion resistance target because of the thermal modifications induced by laser processing. This difference is due to the presence of a residual HAZ after laser cutting and post-processing, which changes the material properties.

### 4.4. *Prototyping and applications*

Because of its extraordinary properties, Nitinol is widely employed in many industrial sectors, such as the automotive, aerospace, and biomedical industries. Laser processing enables the realisation of microdevices, such as stents, catheters, dampers, sensors, and actuators, which are vastly implemented in the medical, automotive, and aeronautical fields. After laser processing, the properties may change; hence, the material could require post-processing to recover them [43,89]. The following subsections discuss the main categories of applications of NiTi SMAs processed by laser cutting.

#### 4.4.1. *Biomedical devices*

Among the fields of application of SMAs, biomedicine was the first sector capable of applying the functional performances of NiTi alloys in advanced devices, mainly because of their biocompatibility, corrosion resistance, and SE.

The most diffused and well-known device processed via laser cutting is the stent, which has been mentioned several times in the present paper.

Favier studied the effect of two stent cutting methods, based on the expansion of the patterned cut on a small tube or by cutting the mesh on the tube of larger diameter, on the transformation temperatures of the MT, detected by DSC measurements [27]. It was found that the pre-cut stents exhibited less homogeneity in the MT of the pre-expanded stents. This is due to the stress distribution induced by the stent bending, which can promote less homogeneity in the material.

Frotscher et al. reported the processing and functional characterisation of braided NiTi stents [24]. In particular, they compared laser cutting and braiding for producing microstents. Although laser cutting can offer high precision and high spatial resolution, as well as thermal modifications, the braiding of very thin wires, down to 20 μm in diameter, could be considered a promising technology. Fig. 33 summarises the principal mechanical performances of both the stent types, processed via laser cutting and the braiding method. No difference was observed between the two types of stents in the

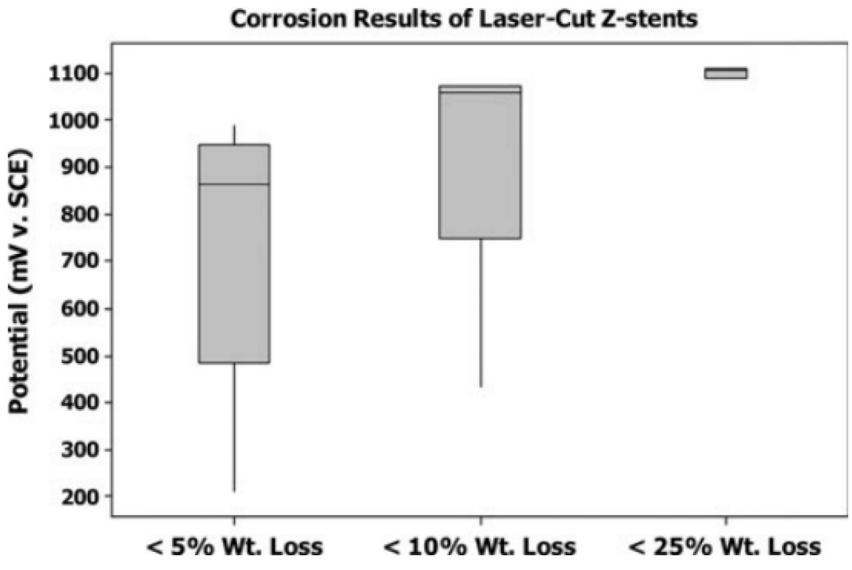


(a)

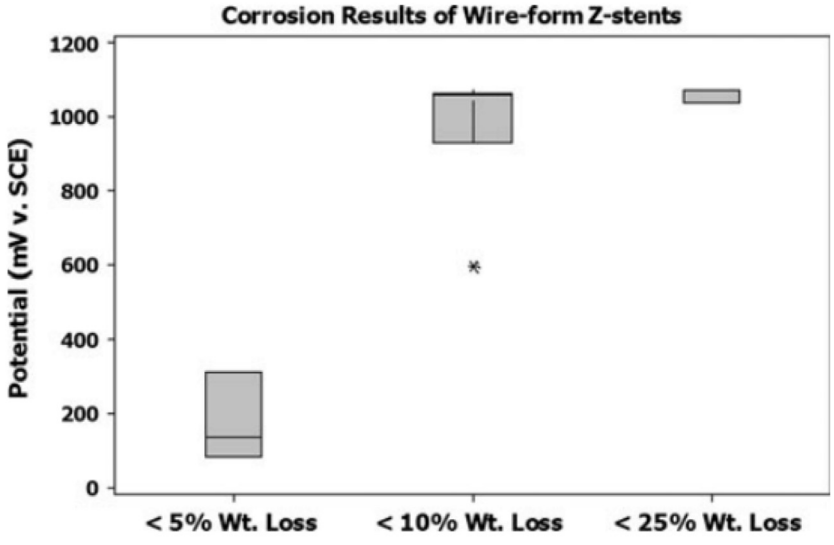


(b)

**Fig. 32 – Corrosion results as functions of the weight loss in the (a) laser-cut and (b) wire-formed stents [88].**

first millimetre of displacement. At higher displacements, the braided stents showed a steep load increase, whereas the laser-cut stent exhibited a much less pronounced load increase (see Fig. 33a). Fig. 35b presents the results of 20 loading–unloading cycles performed at 37 °C with less than 4 mm maximum displacements on both types of stents. The load-displacement curve of the braided stent was bent upward, whereas that of the laser-cut stent showed higher deformability under low applied loads. The maximum loads applied during the fatigue cycling of the braided and laser-cut stents were approximately 0.1 and 0.25 N, respectively. These values did not change significantly during cycling (Fig. 33c). However, the maximum loads of the laser-cut stents remained constant, whereas those of the braided stents slightly decreased after two million cycles.

The surface of the laser cut stent is a relevant issue; some works were dedicated to the post-processing [84]. In details, acid pickling, being one of the major methods to remove the

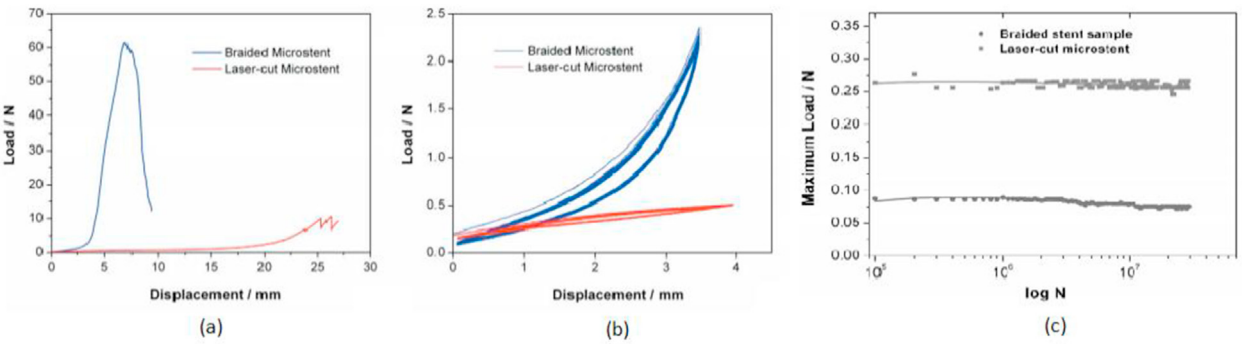


**Fig. 33 – (a) Mechanical response at failure, (b) loading–unloading cycling, and (c) fatigue behaviour of NiTi stents [24].**

burr and the depositions, was tested for cleaning laser cut stents.

It is important to avoid carefully the generation of thermal defects during laser machining, which would produce local stress concentrations that could cause the component to fail [90]. Therefore, finite element modelling of laser-cut stent coupons can support stress distribution analysis and identification of the most critical points at which failure can occur, as shown in Fig. 34. The corresponding Wohler curve representing the fatigue behaviour of the coupon in NiTi indicates a combination of stress, strain, and life cycles that satisfies the stent requirements. The stents tested with an alternative strain of 1% could resist any breaks (indicated as run-out) up to $10^7$ cycles (see Fig. 35).

Another biomedical device involving NiTi is dedicated to surgical tooling. In neurosurgery, the simultaneous use of two instruments through the same endoscopic shaft is a complex issue. An endoscopic shaft contains channels for the optic element, rinsing system, and small-diameter instruments, such as handles, shafts, and actuators for controlling the attached head (graspers and scissors). There are some issues related to the manipulation and control of these instruments, and the design and realisation of complex steerable instruments with the required small diameters is challenging. Dewaele et al. demonstrated the use of laser cutting for the manufacturing of shaped superelastic NiTi elements for steerable instruments, improving the ability to work simultaneously with two tools [91]. A wrist-like element, placed at the distal end of the instrument, was designed to enhance the performance in surgery. Laser cutting of thin NiTi tubes enabled the manufacturing of small-diameter instruments with a large open lumen and excellent tip stability.

Another type of NiTi device applied in the biomedical sector is the small-diameter hydraulic active bending catheter [92,93]. Catheter-based minimally invasive diagnoses and therapy of blood vessels are widely performed. In the related works, the authors proposed the realisation of a superelastic NiTi tube, processed by laser cutting (see Fig. 36a) and inserted

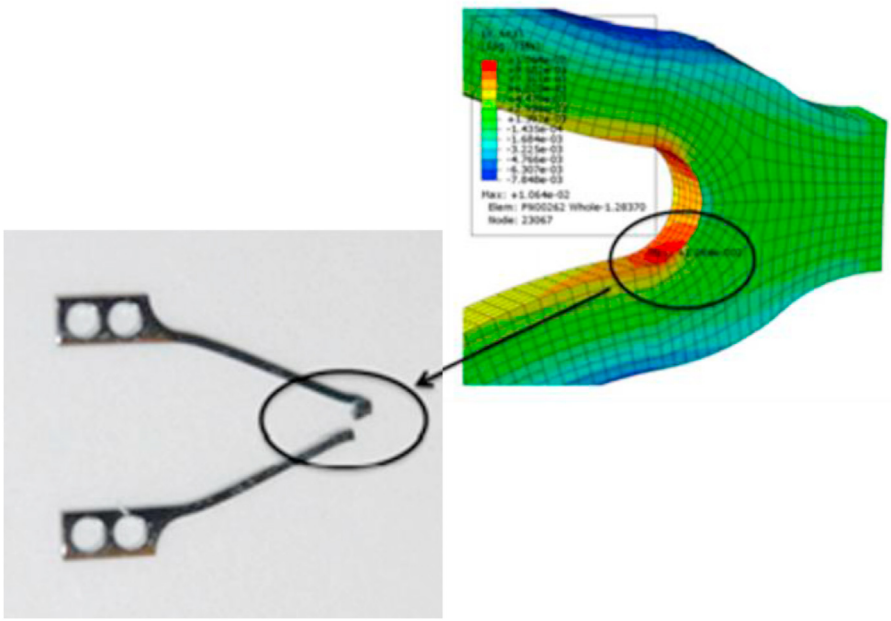

**Fig. 34 – FEM of a NiTi coupon and tested coupon at failure [90].**

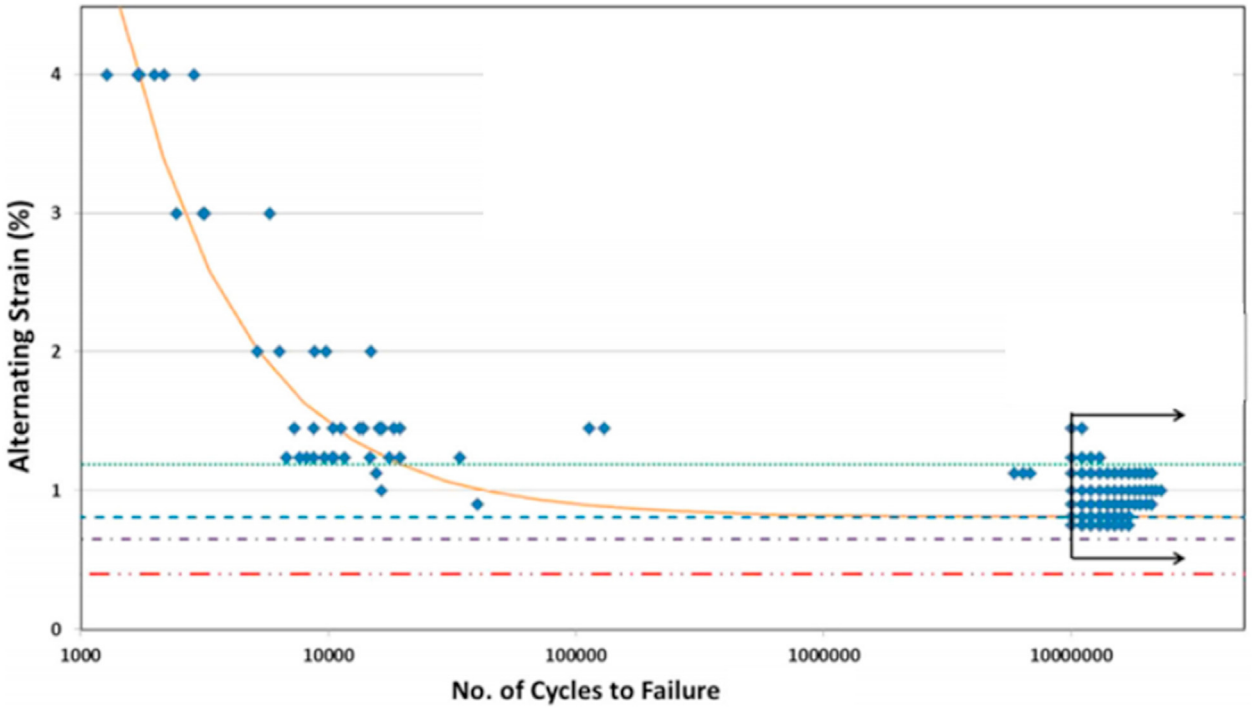


**Fig. 35 – Wohler curve representing the fatigue behaviour of the coupon in NiTi [90].**

it into a silicone rubber tube. This prototype active catheter was filled with water, and its bending angle was actuated from outside the body by suction of the water. Fig. 36b shows the functional response of the catheter, in which the correlation between the water pressure and bending angle is highlighted, and Fig. 36c and 3d present pictures of the catheter bent into the two extreme positions.

#### 4.4.2. *Actuators*

From a scientific perspective, actuators, or more precisely micro- or mini-actuators, based on SMEs represent the most investigated application of SMAs. The functional properties of SMAs enable the realisation of actuators, which change shape with temperature variation. Three approaches have been reported for the realisation of NiTi SMA actuators: the use of 2D and 3D laser cutting to produce planar and tubular shapes and the deposition of thin films on a substrate.

By utilising the SME on 2D laser-cut elements, it is also possible to develop micro-grippers: actuation can be achieved by coupling two actuation units, controlled by electrical heating, to generate mechanical work. The antagonist mechanism is crucial for the device design. Generally, the elements designed with Nitinol are very small, and the generation of optimal gripper element shapes is essential.

However, the actuation speed must be quite high to suit the specific application for which it is developed, and the market has moved towards micro-actuators, which provide faster actuation and larger forces compared to their dimensions [43]. The fabrication method of micro-devices is critical, and it has been observed that fabricating actuators from cold-rolled NiTi sheets generates anisotropies caused by the rolling direction, even after heat treatment for shape memory optimisation. Moreover, it has been observed that, for devices of different thicknesses, with small thickness changes, the transformation temperatures change only if the device works in the direction transverse to the rolling [94]. In addition, in the most common actuation application in which the material only remembers two positions (in the martensitic and austenitic phases), a third position may be generated in the material without any additional control system, increasing its potential for utilisation. Kohl et al. studied the functional performance of microgrippers for robotic applications, as shown in Fig. 37. The presented design consisted of two integrated actuation units with opposite motion directions to separate the control during the opening and closing motions. The response times of the actuation units upon heating were investigated by performing time-resolved electrical resistance measurements. Upon heating, the electrical resistance decreased and finally reached a minimum, which coincided with the end position of the corresponding displacement. The increase in the electrical power decreased the response times. The cooling times were considerably longer, on the order of 300 ms (corresponding to an electrical power of 22 mW) and had no influence on the response times.

The diversity of complex shapes achievable using laser cutting has been exploited to produce various actuators. The active elements of the actuators have utilised NiTi SMA components, which have been integrated into the final device structure. For instance, Garces-Schroder et al. proposed the realisation of silicon microgrippers using integrated NiTi elements produced by ultrashort laser cutting [95]. A hybrid novel wafer-level assembled in-plane SMA actuator and silicon

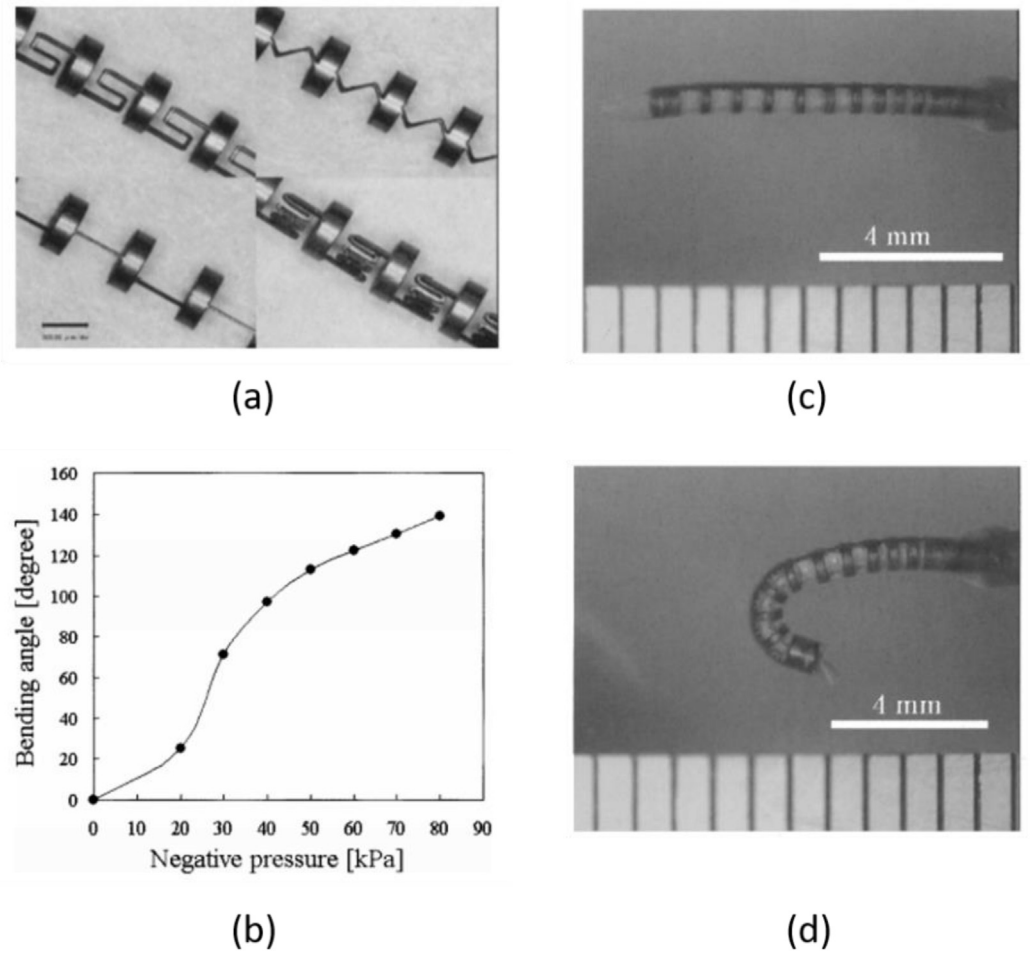


**Fig. 36 – (a) Laser-cut NiTi tubes, (b) functional behaviour of the catheter, (c) catheter before bending, and (d) catheter after bending at the extreme angle [93].**

microgrippers were developed and tested (see Fig. 38). Similar NiTi structures have been realised by other groups to realise actuators operating under different functional conditions. Leester-Schadel et al. reported some prototypes for different sectors: a highly adaptable multi-actuator system for active shape control, micro-gripper for handling microdevices, and micro-actuator for the guidance of surgical resection instruments [45].

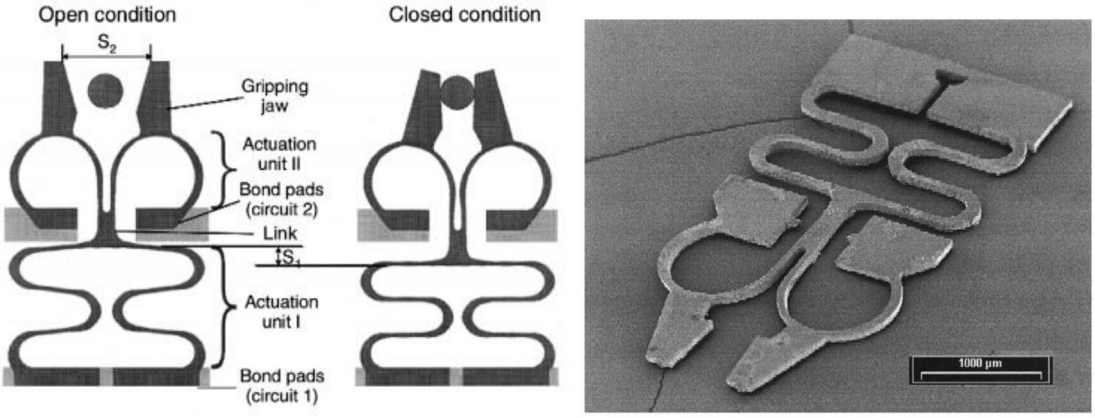


**Fig. 37 – (a) Schematic showing the operation principle of the SMA micro-gripper and (b) the laser-cut Nitinol element [94].**

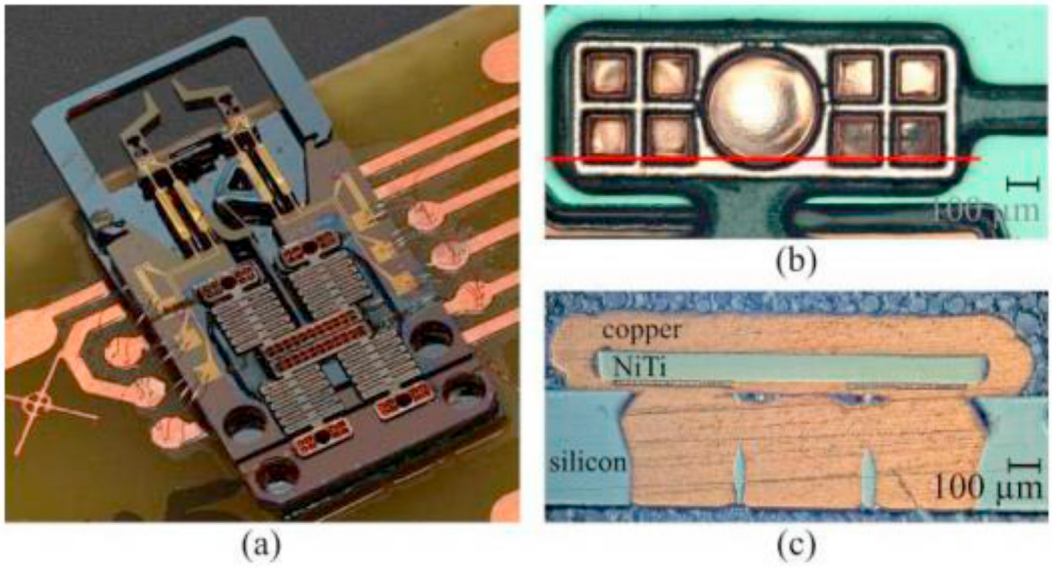


**Fig. 38 – (a) Microgripper with NiTi SMA actuator mounted on a printed circuit board and force sensors contacted by wire bonds for force sensor characterization, (b) micrograph of rivet connection of gripper and actuator, and (c) cross-section of rivet connection [95].**

Regarding the realisation of 3D SMA actuators, Tian et al. studied different structures designed for actuating continuum robots [96]. Starting from thin-walled tubes in superelastic NiTi SMA, the laser cutting process was selected for processing spiral-shaped structures, such as spindle apparatus, peanut, and spiral structures, as depicted in Fig. 39. Single- and multi-segment prototypes exhibited promising motion ability in terms of flexural rigidity and continuous deformation. Such prototypes can offer enhanced performance and work capabilities of continuum robots in confined spaces, as indicated by the functional response presented in Fig. 40. In fact, finite element modelling highlighted that these spiral structures could undergo large deformations without evident stress concentrations.

Tung et al. designed and realised NiTi elements for active steerable catheters, starting from thin-walled tubes [89,97]. Tubular 3D actuators were designed for manipulation inside human blood vessels, and their functional behaviour was modelled using the FEM. The laser-machined actuator showed similar performance to the SMA wire actuator with comparable transition temperature in quasi-static testing, although neither actuator exhibited the same stress plateau characteristics as the superelastic wire [89]. In this work, no post-processing was performed; therefore, some actuators broke under undesirable conditions, but this drawback can be overcome by performing electropolishing. In contrast, the dynamic characterisation data showed that the ability of the actuator to recover 32% of its length was within the range required for the considered application. The fatigue properties seemed to be relatively stable, although it took several cycles for the displacement to settle [97].

The practical use of the proposed actuators in active catheters requires the consideration of cooling because the temperatures reached during thermal actuation can cause tissue damage. However, as these actuators have very low

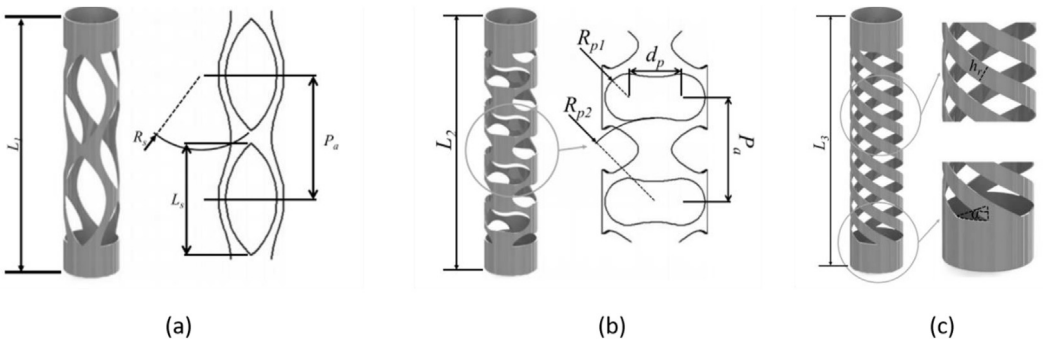


**Fig. 39 – Different types of spiral support structures in NiTi SMA: (a) spindle apparatus, (b) peanut, and (c) spiral structure [96].**

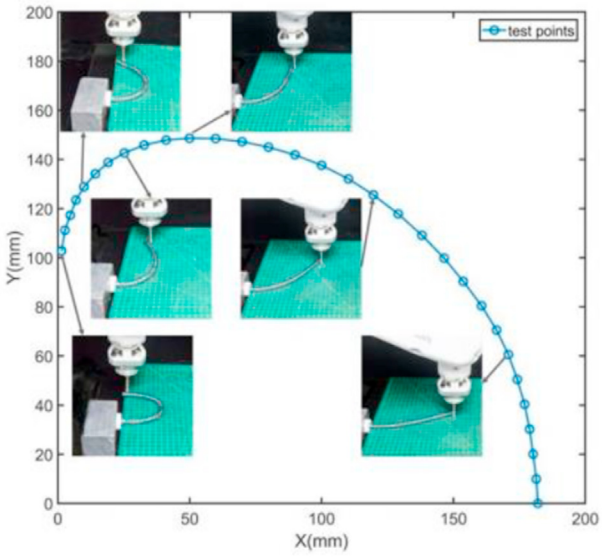


**Fig. 40 – Motion trajectory of the force-bearing point of a multi-segment NiTi prototype [96].**

thermal masses, both blood flowing outside the catheter and active cooling inside should help to mitigate this drawback.

Finally, as shown by Huang et al. [98,99] on a cantilever, this can be obtained by coupling Nitinol with another material, such as Si, owing to the uneven temperature distribution in the element. The Si substrate with NiTi coating was laser cut in the middle of the cantilever, which is flat at ambient temperature but becomes curved upon heating.

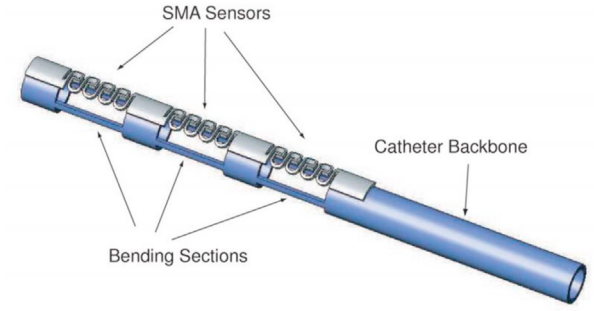


(a)

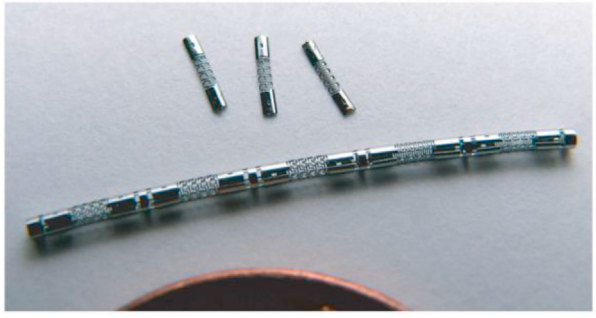

(b)

**Fig. 41 – (a) Schematic of a NiTi SMA sensor mounted on a SMA backbone used as an active catheter and (b) pictures of laser-cut sensors [100].**

#### 4.4.3. *Sensors*

Based on the opposite principle of SMA actuator operation, superelastic NiTi sensors can be realised using laser cutting and electro-polishing to control the positions of some elements. Tung proposed a sensor for surgical applications, as shown in Fig. 41 [100]. They found that the signal output could be altered and the stiffness of the sensors could be reduced by varying the dimensional features of the elements.

With proper amplification and compensation, NiTi sensors have been characterised by low root-mean-square error and drift and can function as linear position sensors, especially when used differentially. The proposed path can enable the practical use of SMA materials, especially in active catheters, and ultimately improve medical devices and benefit patient care.

#### 4.4.4. *Dampers*

Small-amplitude and passive vibration damping can be important in mechanical applications, where random broadband excitations are present in a typical operational environment. NiTi-based SMAs also offer high damping capacity [101], which can be exploited to realise dampers for vibration suppression. Composite structures containing some NiTi SMA wires were realised with promising damping performance [102]. To improve the fabrication method and composite performance, the SMA wires were replaced by thin sheets of NiTi-based SMA, shaped by laser cutting, and inserted into the resin panel, as shown in Fig. 42. Different ellipsoidal paths were laser-cut with a nanosecond fibre laser from Ni40Ti50Cu10 SMA tapes with thicknesses of 0.15 mm. The flexural damping behaviour of the sandwich-structured composite panel was tested experimentally in the flexural mode, and finite element modelling was performed to determine the stress distribution [46,47,103].

The damping coefficient h was found to be directly proportional to the amount of SMA, as shown in Fig. 43. As the pure resin can offer only a damping value in the range 0.4–0.45, the use of SMA sheets can significantly improve the vibration suppression capability, and the increase in the quantity of SMA from large to small ellipsoidal paths increases the damping behaviour from 0.45 to 0.6. According to these findings, composites with embedded uncut sheets can achieve the highest damping performance, but a delamination effect can also occur because of the lack of adhesion between the sheets and resin.

The damping capacity of the composite beam was improved when the NiTiCu alloy was replaced with CuZnAl SMA [104]. The laser cutting of CuZnAl thin sheets induced local compositional variation due to Zn evaporation, which should be added to the typical HAZ. Therefore, the border of the kerf was subjected to functional modification that was more intense than that typically observed for NiTi SMAs. Despite this drawback, this alloy promoted a higher damping capacity, enabling the realisation of composite beams suitable for passive vibration suppression.

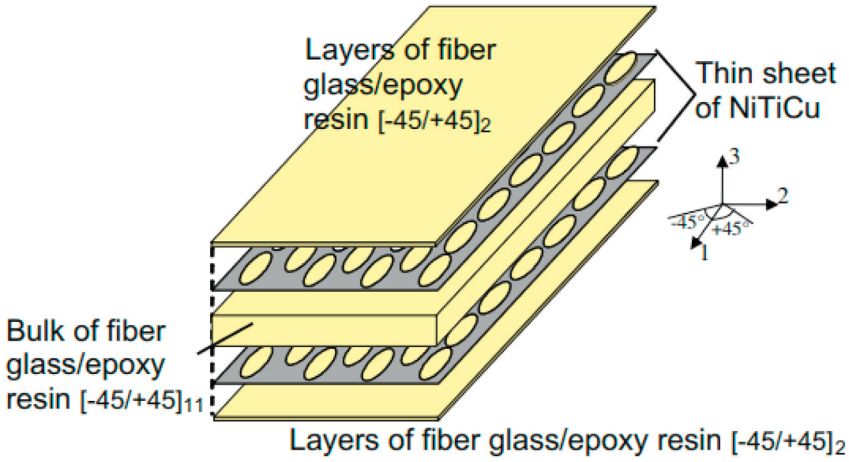


**Fig. 42 – Schematic of a hybrid NiTi-based SMA composite with enhanced damping capacity for vibration suppression [103].**

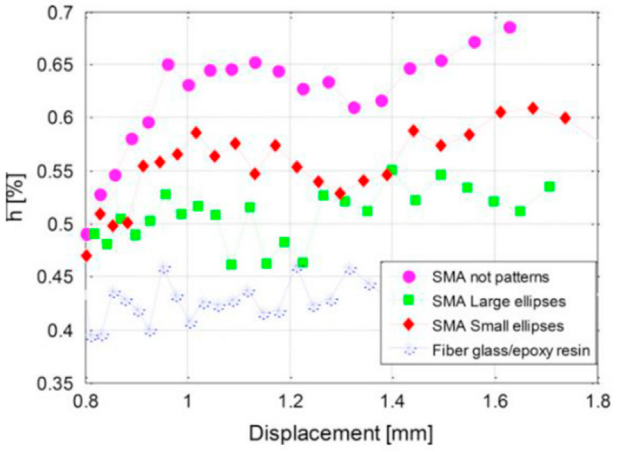


**Fig. 43 – Damping coefficient evaluated for different NiTi-based SMA composite beam configurations [103].**

## 5. Conclusions

Laser processing is among the most widespread technologies for manufacturing NiTi SMA mini- and micro-devices for both industrial and scientific applications. The present report provided a review of the literature regarding the laser cutting process of NiTi SMAs. This topic was discussed from different perspectives, such as technological, metallurgical, and functional approaches, with a particular focus on laser-cut devices for various applications.

The principal conclusions can be highlighted, as in the following:

- NiTi SMAs are very sensitive to temperature changes, therefore the most important parameters of the laser cutting process, such as pulse duration and emission wavelength, can significantly affect the conduction of the heat, consequently the quality of the cut edge. The adoption of ultrashort lasers or hybrid processes, like water jet guided laser beam cutting and cutting under liquid immersion, can promote the best quality of the SMA device. Moreover, the formation of dross, spatter, and kerf irregularities can be also optimised by selecting the optimal process parameters, like power, scanning speed, repetition rate, gas type and flow.
- Thermal modelling of NiTi laser cutting can offer relevant inputs for supporting the design of the laser process. Also in this case, the estimation of the extension of the heat affected zone and melted zone are considered the most promising variables to be analysed.
- The microstructural transformations induced locally by the laser beam can tune the local functional performance of the SMA. This effect can be controlled by reducing largely the laser pulse durations. However, post-processing can also be conducted for removing the altered material, which can influence the functional behaviour of the SMA device, like mechanical and thermal fatigue performances as well as transformation temperatures.
- The realization of several devices and prototypes was also analysed for demonstrating how the large scale possibility of using smart and functional materials, like SMAs, can promote innovative, high tech and advanced components, to be integrated in complex devices, (like sensors, actuators or dampers for different sectors) or components standing alone (like stents for the biomedical sector).

It can be concluded that the use of the laser beam in cutting of NiTi SMA parts is a precise tool, able to readjust its characteristics for improving more and more its performances. Nowadays, several types of stents, and not only these, are completely industrialized, despite the ongoing evolution of the laser technology in the field of the laser material processing.

## Declaration of Competing Interest

The authors declare that they have no known competing financial interests or personal relationships that could have appeared to influence the work reported in this paper.

## Acknowledgements

The authors would like to thank Marco Bonfanti, Karthik Mathivanan, and Matteo Del Nero from Politecnico di Milano. The authors would like to acknowledge Accordo Quadro CNR/Regione Lombardia n. 3866 FHfFC for their financial support.

## REFERENCES

[1] Ready JF, Larson DF. LIA handbook of laser materials processing. Laser Institute of America, Magnolia Publishing; 2001. p. 715. Inc.
[2] Dubey AK, Yadava V. Laser beam machining—a review. Int J Mach Tool Manufact 2008;48:609–28.
[3] Mishra S, Yadava V. Laser beam micro machining (LBMM) – a review. Opt Laser Eng 2015;73:89–122.
[4] Wayman CM, Duerig TW. An introduction to martensite and shape memory, engineering aspects of shape memory alloys. 1990. p. 3–20.
[5] Otsuka K, Ren X. Physical metallurgy of Ti-Ni-based shape memory alloys. Prog Mater Sci 2005;50–5:511–678.
[6] Jani JM, Leary M, Subic A, Gibson MA. A review of shape memory alloy research, applications and opportunities. Mater Des 2014;56:1078–113.
[7] Elahinia MH, Hashemi M, Tabesh M, Bhaduri SB. Manufacturing and processing of NiTi implants: a review. Prog Mater Sci 2012;57:911–46.
[8] Manjaiah M, Narendranath S, Basavarajappa S. Review on non-conventional machining of shape memory alloys. Trans Nonferrous Metals Soc China 2014;24:12–21.
[9] Markopoulos AP, Pressas IS, Manolakos DE. A review on the machining of nickel-titanium shape memory alloys. Rev Adv Mater Sci 2015;42:28–35.
[10] Melton KN. Ni-Ti based shape memory alloys. In: Engineering aspects of shape memory alloys; 1990. p. 21–35.
[11] Tuissi A, Bassani P, Mangioni A, Toia L, Buttera F. Fabrication process and characterization of NiTi wire for actuators, SMST 2004. In: Proc. int. conf. shape memory and superelastic technologies; 2005. p. 501–8.
[12] Favier D, Liub Y, Orgéas L, Sandel A, Debovea L, Comte-Gaz P. Influence of thermomechanical processing on the superelastic properties of a Ni-rich Nitinol shape memory alloy. Mater Sci Eng A 2006;429:130–6.
[13] Li Y, Li JY, Liu M, Ren YY, Chen F, Yao GC, et al. Evolution of microstructure and property of NiTi alloy induced by cold rolling. J Alloys Compd 2015;653:156–61.
[14] Maletta C, Furgiuele F. 1D phenomenological modeling of shape memory and pseudoelasticity in NiTi alloys. In: Smart actuation and sensing systems - recent advances and future challenges; 2012. p. 122–44.
[15] Hodgson DE, Wu MH, Biermann RJ. Shape memory alloys. In: ASM handbook, vol.2; 1990. p. 897–902.
[16] Duerig T, Pelton A, Stockel D. An overview of nitinol medical applications. Mater Sci Eng A 1999;273–275:149–60.
[17] Shabalovskaya SA. Surface, corrosion and biocompatibility aspects of Nitinol as an implant material. Bio Med Mater Eng 2002;12(1):69–109.
[18] Madarati AA, Sammani AMN, Zafar MS, Bani-Younes H, Ahmed HMA. Usage of NiTi rotary instruments for root canal retreatment procedures: experience and practice of dental practitioners and endodontists. ENDO - Endod Pract Today 2016;10(4):213–23.
[19] Pfeifer R, Herzog D, Hustedt M, Barcikowski S. Pulsed Nd-YAG laser cutting of NiTi shape memory alloys—influence of process parameters. J Mater Process Technol 2010;210:1918–25.
[20] Wang W, Fang C, Liu J. Large size superelastic SMA bars: heat treatment strategy, mechanical property and seismic application. Smart Mater Struct 2016;25(7):075001.
[21] Frenzel J, George EP, Dlouhy A, Somsen Ch, Wagner MF-X, Eggeler G. Influence of Ni on martensitic phase transformations in NiTi shape memory alloys. Acta Mater 2010;58(9):3444–58.
[22] Stoeckel D, Pelton A, Duerig T. Self-expanding nitinol stents:material and design considerations. Eur Radiol 2004;14:292–301.
[23] Melzer A, Stoeckel D. Function and performance of nitinol vascular implants. Open Med Dev J 2010;2:32–41.
[24] Frotscher M, Schreiber F, Neelakantan L, Gries T, Eggeler G. Processing and characterization of braided NiTi microstents for medical applications. Matwiss Werkstofftech 2011;42(11):1002–12. https://doi.org/10.1002/mawe.201100796.
[25] Domingo S, Puértolas S, Gracia-Villa L, Mainar M, Usón J, Puértolas JA. Design, manufacture and evaluation of a NiTi stent for colon obstruction. Bio Med Mater Eng 2005;15(5):357–65. 2005.
[26] Stoeckel D, Pelton A, Duerig T. Self-expanding Nitinol stents- material and Design considerations. Proc Eur Radiol 2003;14(2):292–301.
[27] Favier D, Orgéas L, Ferrier D, Poncini P, Liu Y. Influence of manufacturing methods on the homogeneity and properties of Nitinol tubular stents. J Phys 2000;11:541–6.
[28] Zainal MA, Sahlan S, Ali MSM. Micromachined shape-memory alloy microactuators and their application in biomedical devices. Micromachines 2015;6:879–901.
[29] Kohl M. Shape memory microactuators. Microtechnology and mems. 2004. p. 45–9.
[30] Nespoli A, Besseghini S, Pittaccio S, Villa E, Viscuso S. The high potential of shape memory alloys in developing miniature mechanical devices: a review on shape memory alloy mini-actuators. Sens Actuators A 2010;158:149–60.
[31] Nespoli A, Biffi CA, Casati R, Villa E, Tuissi A, Passaretti F. In: Berselli Giovanni, Vertechy Rocco, Vassura Gabriele, editors. New developments on mini/micro shape memory actuators. Smart actuation and sensing systems - recent advances and future challenges; 2012. p. 35–51. ISBN 978-953-51-0798-9.
[32] Fang C, Yam MCH, Lam ACC, Xie L. Cyclic performance of extended end-plate connections equipped with shape memory alloy bolts. J Constr Steel Res 2014;94:122–36. https://doi.org/10.1016/j.jcsr.2013.11.008. ISSN 0143-974X.
[33] Fang H, Wang W, He C, Chen Y. Self-centring behaviour of steel and steel-concrete composite connections equipped with NiTi SMA bolts. Eng Struct 2017;150:390–408. https://doi.org/10.1016/j.engstruct.2017.07.067. ISSN 0141-0296.
[34] Hermawan Hendra, Mantovani Diego. Process of prototyping coronary stents from biodegradable Fe–Mn alloys. Acta Biomater November 2013;9(10):8585–92.
[35] Hung Chia-Hung, Chang Fuh-Yu. Curve micromachining on the edges of nitinol biliary stent by ultrashort pulses laser. Opt Laser Technol 2017;90:1–6. https://doi.org/10.1016/j.optlastec.2016.10.018. ISSN 0030-3992.
[36] Meng Hongyun, Liao Jianhong, Zhou Yongheng, Zhang Qingmao. Laser micro-processing of cardiovascular stent with fiber laser cutting system. Opt Laser Technol 2009;41:300–2.
[37] Strobel M, Schuessler A. Status and trends in laser micromachining of metallic medical components. In:

Proceesings of th international conference on shape memory and superelastic technologies; 2004. p. 287–2293.
[38] Rae Kim Won, Bae Bang Gyung, Hyun Park Jung, Lee Taeg Woo, Lee Byoung-Soo, Yang Seung-Min, et al. Microstructural study on a Fe-10Cu alloy fabricated by selective laser melting for defect-free process optimization based on the energy density. J Mater Res Technol 2020;9(6):12834–9. https://doi.org/10.1016/j.jmrt.2020.09.051.
[39] Assuncao E, Williams V. Comparison of continuous wave and pulsed wave laser welding effects. Opt Laser Eng 2013;51:674–80.
[40] Meijer J. Laser beam machining (LBM), state of the art and new opportunities. J Mater Process Technol 2004;149:2–17.
[41] Phillips KC, Ganghi HH, Mazur E, Sundaram SK. Ultrafast laser processing of materials:a review. Adv Opt Photon 2015;(4):7. https://doi.org/10.1364/AOP.7.000684.
[42] Muhammad N, Whitehead D, Boor A, Oppenlander W, Liu Z, Li L. Picosecond laser micromachining of nitinol and platinum-iridium alloy for coronary stent applications. Appl Phys A 2012:607–17. 6609-4.
[43] Rohde M, Schüssler A. On the response-time behaviour of laser micromachined NiTi shape memory actuators. Small 1997;61:463–8. https://doi.org/10.1016/S0924-4247(97)80306-8.
[44] Kohl M, Krevet B, Just E. Sensors Actuat A 2002;97–98:646–52.
[45] Leester-Schädel M, Hoxhold B, Lesche C, Demming S, Büttgenbach S. Micro actuators on the basis of thin SMA foils. Microsyst Technol 2008;14:697–704. https://doi.org/10.1007/s00542-008-0600-9.
[46] Arnaboldi S, Bassani P, Biffi CA, Tuissi A, Carnevale M, Lecis N, et al. Simulated and experimental damping properties of a SMA/Fiber glass laminated composite. J Mater Eng Perform 2011;20:551–8. https://doi.org/10.1007/s11665-011-9887-2.
[47] Biffi CA, Bassani P, Tuissi A, Carnevale M, Lecis N, LoConte A, et al. Numerical and experimental characterization of damping properties of SMAs composite for vibration control systems. J Mater Eng Perform 2012. https://doi.org/10.1007/s11665-012-0293-1. ISSN 1059-9495.
[48] Lin HC, Lin KM, Chen YC. The laser machining characteristics of TiNi shape memory alloys. High Temp Mater Process 1999;3:409–20.
[49] Schüssler A., Laser processing of Nititol material, SMST 2000. Proceedings of the International Conference on Shape memory and Superelastic Technologies.
[50] Previtali B, Arnaboldi S, Bassani P, Biffi CA, Lecis N, Tuissi A, et al. Microcutting of NiTiCu alloy with pulsed fiber laser, ESDA2010-24943. In: 10th biennial conference on engineering systems design and analysis, Esda 2010, July 12-14. Turkey: Istanbul; 2010.
[51] Dickson TR, Moore B, Toyama N. Innovations: laser-cutting nickel-titanium. Mater Sci Forum 2002;394–395:309–12.
[52] Rao BT, Kaul R, Tiwari P, Nath AK. Opt Laser Eng 2005;43:1330–48.
[53] Biffi CA, Tuissi A. Nitinol laser cutting: microstructure and functional properties of femtosecond and continuous wave laser processing. Smart Mater Struct 2017;26:35006. https://doi.org/10.1088/1361-665X/aa5596.
[54] Fu CH, Liu JF, Guo A. Statistical characteristics of surface integrity by fiber laser cutting of Nitinol vascular stents. Appl Surf Sci 2015;353:291–9. https://doi.org/10.1016/j.apsusc.2015.06.105.
[55] Fu CH, Liu JF, Guo YB, Zhao QZ. A comparative study on white layer properties by laser cutting vs electrical discharge machining of Nitinol shape memory alloy. In: 18th CIRP conference on electro physical and chemical machining, procedia CIRP, vol. 42; 2016. p. 246–51.
[56] Liu L, Bo D, Yi L, Tong F, Fu Y. Fiber laser micromachining of thin NiTi tubes for shape memory vascular stents. Appl Phys A 2016;122:1–9. https://doi.org/10.1007/s00339-016-0170-0.
[57] Nagy P, Dobranszky J. Laser cutting of small diameter nitinol tube. Mater Sci Forum 2013;729:460–3.
[58] Momma C, Knop U, Nolte S. Laser cutting of slotted tube coronary stents - state of the art and future developments. Prog Mater Sci 1999:39–44.
[59] Stolberg K, Friedel S, Kremser B, Roehner M. IR and green femtosecond laser machining of heat sensitive materials for medical devices at micrometer scale. Proc SPIE 2014;8968:89680E.
[60] Yang Y, Yang J, Liang C, Wang H, Zhu X, Kuang D, et al. Sub-wavelength surface structuring of NiTi alloy by femtosecond laser pulses. Appl Phys A 2008;92:635–42.
[61] Liang C, Wang H, Yang J, Li B, Yang Y, Li H. Biocompatibility of the micro-patterned NiTi surface produced by femtosecond laser. Appl Surf Sci 2012;261:337–42.
[62] Nozaki K, Shinonaga T, Ebe N, Horiuchi N, Nakamura M, Tsutsumi Y, et al. Hierarchical periodic micro/nano-structures on nitinol and their influence on oriented endothelialisation and anti-thrombosis. Mater Sci Eng C 2015;57:1–6.
[63] Huang H, Zheng HY, Lim GC. Femtosecond laser machining characteristics of Nitinol. Appl Surf Sci 2004;228:201–6. https://doi.org/10.1016/j.apsusc.2004.01.018.
[64] Li C, Nikumb S, Wong F. An optimal process of femtosecond laser cutting of NiTi shape memory alloy for fabrication of miniature devices. Opt Laser Eng 2006;44:1078–87.
[65] Uppal N, Shiakolas PS. Micromachining characteristics of NiTi based shape memory alloy using femtosecond laser. J Manuf Sci Eng 2008;130:31117. https://doi.org/10.1115/1.2936380.
[66] Quintino L, Liu L, Miranda RM, Silva RJC, Hu A, Zhou Y. Cutting NiTi with femtosecond laser. Adv Mater Sci Eng 2013;2013. https://doi.org/10.1155/2013/198434.
[67] Hung CH, Chang F-Y, Chang T-L, Chang Y-T, Huang K-W, Liang P-C. Femtosecond laser nonlinear ablation process of biliary nitinol stent for cholangiocarcinoma. Adv Mater Res 2013;699:859–63.
[68] Hung C-H, Chang F-Y, Chang T-L, Chang Y-T, Huang K-W, Liang P-C. Micromachining NiTi tubes for use in medical devices by using a femtosecond laser. Opt Laser Eng 2015;66:34–40. https://doi.org/10.1016/j.optlaseng.2014.08.001.
[69] Huang H, Zheng HY, Liu Y. Experimental investigations of the machinability of Ni 50.6 Ti 49.4 alloy. Smart Mater Struct 2005;14:S297–301. https://doi.org/10.1088/0964-1726/14/5/019.
[70] Muhammad N, Li L. Underwater femtosecond laser micromachining of thin nitinol tubes for medical coronary stent manufacture. Appl Phys A Mater Sci Process 2012;107:849–61. https://doi.org/10.1007/s00339-012-6795-8.
[71] Levesque T, Perrottet D, Richerzhagen B. Damage-free cutting of medical devices using the water-ject-guided laser. In: Proceedings of the materials and processes for medical devices conference; 2006.
[72] Yung KC, Zhu HH, Yue TM. Theoretical and experimental study on the kerf profile of the laser micro-cutting NiTi shape memory alloy using 355 nm Nd:YAG. Smart Mater Struct 2005;14:337–42. https://doi.org/10.1088/0964-1726/14/2/006.
[73] https://www.synova.ch./technology/laser-microjet.htlm.
[74] Fu CH, Guo YB, Sealy MP. A predictive model and validation of laser cutting of nitinol with a novel moving volumetric

pulsed heat flux. J Mater Process Technol 2014;214:2926–34. https://doi.org/10.1016/j.jmatprotec.2014.06.010.
[75] Fu CH, Sealy MP, Guo YB, Wei XT. Finite element simulation and experimental validation of pulsed laser cutting of nitinol. J Manuf Process 2015;19:81–6. https://doi.org/10.1016/j.jmapro.2015.06.005.
[76] MacWilliams J. Optimization of Nitinol shape setting through post laser cutting processing. In: Proceedings of the materials and processes for medical devices conference; 2006.
[77] Toro A, Van Geertruyden W, Misiolek WZ, Han XD, Wu MH. Microstructural characterization of Ni-Ti vascular stents. In: Proceedings of the materials & processes for medical devices conference, November 14-16; 2005.
[78] Tuissi A, Biffi CA, Ruella S, Casati R. High performance shape memory effect (HP-SME) for new shape memory devices: a diamond-like actuator. Mater Today Proc 2015;2:S975–8. https://doi.org/10.1016/j.matpr.2015.07.444.
[79] Miller DA, Lagoudas DC. Influence of cold work and heat treatment on the shape memory and plastic strain development of NiTi. Mater Sci Eng A 2001;308:161–75.
[80] Mitwally M, Farag M. Effect of cold work and annealing on the structure and characteristics of NiTi alloy. Mater Sci Eng A 2009;519:155–66.
[81] Nespoli A, Biffi CA, Previtali B, Villa E, Tuissi A. Laser and surface processes of NiTi shape memory elements for micro-actuation. Metall Mater Trans A 2014;45:1–8. https://doi.org/10.1007/s11661-013-2177-x.
[82] Biffi CA, Nespoli A, Previtali B, Villa E, Tuissi A. Functional response of NiTi elements for smart micro-actuation applications. J Mater Eng Perform 2014;23:2351–6. https://doi.org/10.1007/s11665-014-0898-7.
[83] Biffi CA, Bonacina L, Nespoli A, Previtali B. On the thermo-mechanical behavior of NiTi shape memory elements for potential smart micro-actuation applications. J Intell Mater Syst Struct 2015;27:1–10. https://doi.org/10.1177/1045389X14566521.
[84] Zhao H, Stalmans R, Van Humbeeck J, De Scheerder I. Pickling of laser-cut NiTi slotted tube stents: effect on surface morphology, dimension changes and mechanical behaviour. J Phys IVP 2003;112:1125. 10.1051/jp4:20031080.
[85] Biffi CA, Bassani P, Carnevale M, Lecis N, LoConte A, Previtali B, et al. Effect of laser microcutting on thermo-mechanical properties of NiTiCu shape memory alloy. Met Mater Int 2014;20:83–92. https://doi.org/10.1007/s12540-013-6011-1.
[86] Biffi CA, Tuissi A. Laser shape setting of superelastic NiTi wire: effects of laser beam power and axial pre-load. Smart Mater Struct 2019. https://doi.org/10.1088/1361-665X/ab1e86.
[87] Biffi CA, Mathivanan K, Tuissi A. Laser-induced superelasticity in NiTinol stent strut. Shape Mem Superelasticity 2018;4:377–82. https://doi.org/10.1007/s40830-018-0183-y.
[88] Decker JF, Trépanier C, Vien L, Pelton AR. The effect of material removal on the corrosion resistance and biocompatibility of nitinol laser-cut and wire-form products. J Mater Eng Perform 2011;20:802–6. https://doi.org/10.1007/s11665-011-9882-7.
[89] Tung AT, Park BH, Koolwal A, Nelson B, Niemeyer G, Liang D. Design and fabrication of tubular shape memory alloy actuators for active catheters. In: Proc. first IEEE/RAS-EMBS int. conf. biomed. robot. biomechatronics, 2006, BioRob 2006; 2006. p. 775–80. https://doi.org/10.1109/BIOROB.2006.1639184. 2006.
[90] Forcucci S. Laser cut Nitinol tubing fatigue coupon: design, testing, and endurance limit. J Mater Eng Perform 2014;23:2523–32.
[91] Dewaele F, Kalmar AF, De Ryck F, Lumen N, Williams L, Baert E, et al. A novel design for steerable instruments based on laser-cut nitinol. Surg Innovat 2014;21(3):303–11. https://doi.org/10.1177/1553350613508015.
[92] Haga Y, Muyari Y, Mineta T, Matsunaga T, Akahori H, Esashi M. Small diameter hydraulic active bending catheter using laser processed super elastic alloy and silicone rubber tube. In: 2005 3rd IEEE/EMBS spec. top. conf. microtechnology med. biol.; 2005. p. 245–8. https://doi.org/10.1109/MMB.2005.1548439. 2005.
[93] Haga Y, Muyari Y, Goto S, Matsunaga T, Esashi M. Development of minimally invasive medical tools using laser processing on cylindrical substrates. Electr Eng Jpn (English Transl. Denki Gakkai Ronbunshi) 2011;176:65–74. https://doi.org/10.1002/eej.21030.
[94] Kohl M, Just E, Pfleging W, Miyazaki S. SMA microgripper with integrated antagonism. Sens Actuator A Phys 2000;83:208–13. https://doi.org/10.1016/S0924-4247(99)00385-4.
[95] Garces-Schroder M, Zimmermann T, Siemers C, Leester-Schadel M, Bol M, Dietzel A. Shape memory alloy actuactors for silicon microgrippers. J Microelectromech Syst 2019;28(5).
[96] Tian J, Wang T, Fang X, Shi Z. Design, fabrication and modeling analysis of a spiral support structure with superelastic Ni-Ti shape memory alloy for continuum robot. Smart Mater Struct 2020;29.
[97] Tung AT, Park BH, Niemeyer G, Liang DH. Laser-machined shape memory alloy actuators for active catheters. IEEE ASME Trans Mechatron 2007;12(4).
[98] Huang WM, He Q, Hong MH, Xie Q, Fu YQ, Du HJ. On the fabrication of NiTi shape memory alloy micro devices using laser, vol. 4915; 2002. p. 234–40.
[99] Huang WM, Liu QY, He LM, Yeo JH. Micro NiTi-Si cantilever with three stable positions. Sens Actuator A Phys 2004;114:118–22. https://doi.org/10.1016/j.sna.2004.02.027.
[100] Tung AT, Park B, Liang DH, Niemeyer G. Laser-machined shape memory alloy sensors for position feedback in active catheters. Sens Actuator A Phys 2009;147:83–92. https://doi.org/10.1016/j.sna.2008.03.024.
[101] Van Humbeeck J. Damping capacity of thermoelastic martensite in shape memory alloys. J Alloy Compd 2003;355:58–64.
[102] Tuissi A, Bassani P, Casati A, Bocciolone M, Collina A, Carnevale M, et al. Application of SMA composites in the collectors of the railway pantograph for the Italian high speed train. J Mater Eng Perform 2009;18:612–9.
[103] Bassani P, Biffi CA, Carnevale M, Lecis N, Previtali B, Lo Conte A. Passive damping of slender and light structures. Mater Des 2013;45:88–95. https://doi.org/10.1016/j.matdes.2012.08.044.
[104] Biffi CA, Bassani P, Tuissi A, Carnevale M, Lecis N, LoConte A, et al. Flexural vibration suppression of glass fiber/CuZnAl SMA composite. Funct Mater Lett March 2012;1(5). https://doi.org/10.1142/S1793604712500142.

**Carlo Alberto Biffi** is currently working as a researcher at National Research Council of Italy, Institute of Condensed Matter Chemistry and Technologies for Energy, and he serves as professor under contract at Politecnico di Milano (course "Advanced Manufacturing Processes") since 2010. He received his PhD at Politecnico di Milano at 2009. His main interests focus on laser material processing, like cutting, welding, heat treatment and additive manufacturing, and their effect on microstructure and mechanical properties of different metallic materials (mainly Shape Memory Alloys, Ti and Al alloys). He has published 100

papers in peer-reviewed international journals and he has received more than 700 citations with an H-index of 14.

**Jacopo Fiocchi** is currently working as assistant researcher at National Research Council of Italy, Institute of Condensed Matter Chemistry and Technologies for Energy. He graduated in materials engineering and nanotechnology at Politecnico di Milano in 2015. His research interests lie in physical metallurgy of aluminum alloys, produced by conventional methods and additive manufacturing, as well as development of advanced Shape Memory Alloys. He has published more than 20 papers in international journals, with an H-index of 8.

**Ausonio Tuissi** is currently research director at National Research Council of Italy, Institute of Condensed Matter Chemistry and Technologies for Energy. After graduating in Physics in 1990, he has been researching on innovative metallic materials (hape memory alloys, superconducting materials, metal matrix composites), metallic alloys processing by advanced melting technologies (PAM, VIM, VAR), metal additive manufacturing. He has been principal investigator and scientific responsible of several national and international projects and a number of industrial funded activities. He has been official reviewer of CIVR, PRIN, MISE programs and scientific reviewer of several international sci. journals. He served as elected board member in the American Society of Metals ASM-SMST; the International Union of Vacuum Society IUVSTA. He has been board member of the physical metallurgy board of AIM and board member of AIV national societies. He published more than 200 scientific papers and 4 patents.